This preprint has been submitted to *Lithosphere* for peer review.

Revised timing of Cenozoic Atlantic incursions and changing hinterland sediment sources during southern Patagonian orogenesis

Julie C. Fosdick[1], R.A. VanderLeest[1], J.E. Bostelmann T.[2,3], J.S. Leonard[4], R. Ugalde[5], J.L. Oyarzún[6], and Miguel Griffin[7]

[1]Department of Geosciences, University of Connecticut, 354 Mansfield Road, U-1045, Storrs, CT 06269, USA
[2]Instituto de Ciencias de la Tierra, Facultad de Ciencias, Universidad Austral de Chile, Los Laureles s/n, 5090000, Valdivia, Chile.
[3]Programa de Doctorado en Ciencias Mención Ecología y Evolución, Universidad Austral de Chile, Los Laureles s/n, 5090000, Valdivia, Chile.
[4]School of Earth and Space Exploration, Arizona State University, AZ 85287 USA
[5]PEDECIBA Geociencias, Facultad de Ciencias, Universidad de la República, Iguá 4225, Montevideo, Uruguay
[6]Parque Geo-Paleontológico La Cumbre-Baguales, Ruta 9 km 284, Magallanes, Chile
[7]CONICET—División Paleozoología Invertebrados, Museo de La Plata. Paseo del Bosque s/n, La Plata, Argentina

ABSTRACT

New detrital zircon U-Pb geochronology data from the Cenozoic Magallanes Basin in Argentina and Chile ~51°S establish a revised chronostratigraphy of Paleocene – Miocene foreland synorogenic strata and document the rise and subsequent isolation of hinterland sources in the Patagonian Andes from the continental margin. The upsection loss of zircons derived from the hinterland Paleozoic and Late Jurassic sources between ca. 60-44 Ma documents a major shift in sediment routing due to Paleogene orogenesis in the greater Patagonian-Fuegian Andes. Changes in the proportion of grains from hinterland thrust sheets, comprised of Jurassic volcanics and Paleozoic metasedimentary rocks, provide a trackable signal of long-term shifts in orogenic drainage divide and topographic isolation due to widening of the retroarc fold-thrust belt. Youngest detrital zircon U-Pb ages confirm timing of Maastrichtian – Eocene strata, but require substantial age revisions for overlying Cenozoic basinfill. The upper Río Turbio Formation, previously mapped as Eocene in the published record, records a newly recognized Oligocene (34-26 Ma) marine incursion along the basin margin. We suggest that these deposits are genetically linked to the distal Oligocene-Miocene San Julián Formation along the Atlantic coast via an eastward deepening within the foreland basin system that culminated in the *Juliense* phase of the *Patagonian Sea* incursion in the Southern Andes. The overlying Río Guillermo Formation records onset of tectonically generated coarse-grained detritus ca. 24.3 Ma and a transition to the first fully nonmarine conditions on the proximal Patagonian platform since Late Jurassic time, perhaps signaling a Cordilleran-scale upper plate response to increased plate convergence and tectonic plate reorganization.

INTRODUCTION

Tectonics, climate, and eustasy in convergent plate settings control first-order fluctuations between marine and terrestrial environments along continental margins and the transfer of sediment from orogens to basin depocenters. With the emergence of a new paradigm in the last three decades recognizing dynamic interactions and feedbacks between tectonics and climate (Marshall et al., 1982; Beaumont et al., 1992; Willett, 1999), it is all the more essential to differentiate between their signals in the stratigraphic record. For instance, enhanced tectonism in foreland basin settings can cause crustal load-driven basin subsidence and deepening of marine environments (Flemings and Jordan, 1989; Simpson, 2006). Climate variations and orography influence precipitation and temperature gradients, which in turn effect erosion rates, vegetation cover, and even the location of deformation and drainage divides (Bonnet and Crave, 2003; Rehak et al., 2010; Cruz et al., 2011). Globally, climate modulates the growth and ablation of continental ice sheets and sea level (Miller et al., 2005). Cenozoic marine transgressions are well-studied in terms of sequence stratigraphic models for global sea level change (e.g., Miocene US Atlantic history of Browning et al., 2006) and the dominant control of climatic optima are suitable for passive continental margins. However, in tectonically active, shallow-marine basins resolving the relative contributions of tectonic processes and global eustasy, driven by global mechanisms must be carefully considered (Christie-blick, 1991). For example, work in the Cretaceous interior seaway has demonstrated that tectonism is an important player in controlling parasequence progradation and subsidence (Painter and Carrapa, 2013), in addition to eustatic sea-level variations (Houston et al., 2000; Horton et al., 2004a).

An improved understanding of the controls on subaerial emergence or subsidence of these landmasses is fundamental to evaluating potential linkages between mountain building and climate (e.g., Roe et al., 2008), eustatic sea level changes (Browning et al., 2006), sediment delivery to the oceans (Clift et al., 2001; Sommerfield and Wheatcroft, 2007), and biotic responses to changing ecosystems (Marshall et al., 1982; Sepkoski, 1996; Acosta et al., 2014; Palazzesi et al., 2014; Eronen et al., 2015). Moreover, better knowledge of the dynamic response of sedimentary and tectonic systems is critical to scientific issues of our time, including long-term climate change, biogeochemical fluxes to our lakes and oceans, and conservation of mineral and energy resources. A central requirement to unravel these competing processes is detailed chronology and provenance preserved in the sedimentary basin fill. The appearance of sediment with a diagnostic lithology, age, and/or tectonic terrane association is commonly used to infer timing of source area unroofing and to make paleogeographic, tectonic, or climatic interpretations (e.g., Jordan et al., 1993; Barbeau et al., 2009; Nie et al., 2012). However, a source's decline as a prominent sediment contributor to basin infill – potentially through erosional removal, topographic blocking, or burial – is less commonly preserved in the depositional record. Sediment recycling and weathering of source area can further complicate the cause of a waning source signal (Johnsson and Basu, 1993; Cox et al., 1995; Fosdick et al., 2015; Limonta et al., 2015).

The Patagonian Andes, a high-latitude convergent orogen in South America, provides sediment to the genetically linked Magallanes Basin, which extends ~200 km from a retroarc thrust front to the southern Atlantic Ocean (Fig. 1). This relatively narrow distance results in the eastern Atlantic continental margin in Patagonia that is sensitive to sea level fluctuations driven by dynamic and tectonic loading of the flexural foredeep (Fosdick et al., 2014), variations in sediment flux across the coastal plain, eustasy, and global climate and far-field tectonics. The proximal Patagonian foreland near 51°S remained predominantly deep marine from ca. 100-80 Ma (Natland et al., 1974; Biddle et al., 1986; Romans et al., 2011) followed by basin-filling and shoaling to shallow-marine to marginal continental conditions ca. 78-60 Ma (Macellari et al., 1989; Malumián and Caramés, 1997; Schwartz and Graham, 2015a; Manríquez et al., 2019). This northwestern part of the Magallanes Basin coevolved with a structurally complicated Cenozoic development of the southeastern Magallanes and Malvinas depocenters related to the Fuegian orocline (Ghiglione et al., 2010, 2016) and opening of the Drake Passage between Antarctica and South America (Lagabrielle et al., 2009). Deformation across the Patagonian thrust-belt promoted a general eastward shift of deposition in Paleocene-Miocene time (Fosdick et al., 2011).

Near ~51°S, the proximal Cenozoic Magallanes Basin preserves shelfal facies overlain by near-shore and continental facies. Documented middle Cenozoic transgressions in Patagonia and Tierra del Fuego have been linked to Cenozoic global sea level rise due to climate (Rodríguez Raising, 2010; Malumián and Náñez, 2011) and phases of Andean orogenesis (Fosdick et al., 2011; Bostelmann et al., 2013; Gutiérrez et al., 2017). Most notably, the Oligocene-Miocene 'Patagonian Sea' is recorded as the *Juliense* and *Leonense* phases of shallow marine deposition along much of the Atlantic coast and inland Patagonia (Ameghino, 1906; Parras et al., 2012; Cuitiño et al., 2012). Previous work has suggested that the Patagonian Sea was largely influenced by climate optima and eustatic transgressions (Parras et al., 2012) and tectonics (Dix and Parras, 2014). It is yet undetermined (1) if the early (*Juliense*) inland sea reached the proximal part of the Magallanes Basin, (2) how upland source areas changed during Cenozoic foreland sedimentation, and (3) to what extent these marine phases were driven by tectonic subsidence, changes in upland sediment routing/sediment flux, or eustasy. Differentiating among the relative impacts of these large-scale factors is important for recognizing the effects of external controls, such as global climate transitions, versus internal orogenic wedge dynamics (Dahlen et al., 1984; Willett, 1999) and source to sink connections in the transfer of sediment to the world's oceans.

We present new sediment provenance data and a new chronostratigraphy of Eocene – Miocene strata in the Magallanes (Austral) Basin of southern Patagonia that (1) revise the age of marine incursions and changes in orogenic paleogeography during the transition to nonmarine conditions in southern Patagonia, (2) highlight the rise and subsequent isolation of a major hinterland source area due to basinward development of younger orogenic topography, and (3) suggest recycling of Mesozoic grains from Upper Cretaceous sedimentary rocks, rather than direct sourcing from the Mesozoic batholith.

TECTONIC SETTING & BASIN STRATIGRAPHY

The Upper Cretaceous – Cenozoic Magallanes Basin (Fig. 1) records deposition during structural growth of the Patagonian-Fuegian Andes (Ramos and Ghiglione, 2008; Ghiglione et al., 2010; Romans et al., 2011). Following marine conditions that have generally persisted since Late Jurassic time, the early foreland basin history was predominantly deep-marine, with southward deepening from a narrow continental shelf in the north (Macellari et al., 1989; Malkowski et al., 2013; Sickmann et al., 2018) to bathyal conditions in the south (Biddle et al., 1986). Shoaling of the Upper Cretaceous marine depocenter led to shallow-marine and deltaic sedimentation that persisted until Paleocene time (Macellari et al., 1989; Malumián and Caramés, 1997; Romans et al., 2011; Schwartz and Graham, 2015b; George et al., 2019). Thrust front advancement of the Patagonian retroarc thrust belt promoted an eastward shift of the foreland deposition in Paleocene-Miocene time (Fosdick et al., 2011). The primary sediment sources to the Magallanes Basin include the Mesozoic-Cenozoic Southern Patagonian Batholith and related volcanics, Mesozoic basinal rocks of the Rocas Verdes Basin, and to a lesser extent, Paleozoic metamorphic rocks (Fig. 1). The proximity of the basin to an active magmatic arc throughout its history has resulted in intercalated volcanic ashes and abundant magmatically derived zircons proven useful for assessing controls on sedimentation, with prior focus on the Cretaceous strata (Fildani et al., 2003; Bernhardt et al., 2012; Schwartz et al., 2016; Sickmann et al., 2018).

By middle Cenozoic time or earlier, most low-lying regions of eastern South America were undergoing retreat of marine seaways during uplift of the Andes. In contrast, most of the eastern Patagonian foreland remained largely submerged in shallow marine and transitional depositional environments, with a structurally complicated development of the Magallanes and Malvinas foreland depocenters related to the oroclinal curved plate boundary with the Scotia plate (Ghiglione et al., 2010, 2016) and tectonic separation of Antarctica from South America continents during opening of the Drake Passage (Lagabrielle et al., 2009; Houben et al., 2013). In the Última Esperanza District of the Magallanes Basin, (Chile), Cenozoic strata are disconformable on Maastrichtian tide-influenced shelf-edge deltaic Dorotea Formation (Hünicken, 1955; Biddle et al., 1986; Schwartz and Graham, 2015b; Manríquez et al., 2019). However, the timing and extent of this unconformity and its geologic significance is poorly understood given limited chronology and stratigraphic correlation along the basin axis. In our study area (Fig. 1), the Dorotea Formation is unconformably overlain by the laterally discontinuous Paleocene Cerro Dorotea Formation (Hünicken, 1955; Malumián and Caramés, 1997) and overlying Eocene estuarine and subaqueous deltaic Man Aike/ Río Turbio Formations. (Hünicken, 1955; Otero et al., 2012; Ugalde, 2014; Schwartz and Graham, 2015a). Geological observations in Brunswick Peninsula, Isla Riesco, and Río Figueroa shows that this Paleogene stratigraphic separation decreases southward through Tierra del Fuego, where continuous sedimentation occurred until Miocene time (Olivero and Malumián, 2008; Sánchez et al., 2010).

A key stratigraphic unit within our study area is the Río Turbio Formation, which is characterized by glauconitic shallow-marine to lagoonal sandstone, siltstone, claystone, coquina, and interbedded minable coal seams (Malumián and Caramés, 1997; Rodríguez Raising, 2010; Nullo and Combina, 2011) and fossil assemblages of tropical flora, palynomorphs, and marine invertebrates (Hünicken, 1955; Schweitzer et al., 2012). Debate persists on the depositional age of the Río Turbio Formation, with early biostratigraphic studies reporting Eocene through Miocene (Riccardi and Rolleri, 1980) or exclusively Eocene biozones (Malumián and Caramés, 1997; González Estebenet et al., 2016). This depositional unit records high-latitude organic-rich shallow marine and transitional deposition. Therefore, its age is highly relevant for understanding paleoenvironmental conditions and tectonic influences on sedimentation during past climate optima.

The Río Turbio Formation is unconformably overlain by the Río Guillermo Formation, a mostly fluvial sandstone, conglomerate, and coaly claystone with notable abundant silicified tree trunks preserved in life position (Hünicken, 1955; Malumián and Caramés, 1997; Rodríguez

Raising, 2010; Leonard, 2017). Previous workers have proposed an upper Eocene to early Oligocene age for the Río Guillermo Formation (Malumián et al., 2000; Ramos, 2005; Rodríguez Raising, 2010; Vento et al., 2017). Fluvial sedimentation in the Magallanes Basin was briefly interrupted by a shallow marine incursion, resulting in sandstone and mudstone deposits of the Estancia 25 de Mayo Formation (Cuitiño and Scasso, 2010; Cuitiño et al., 2012) and coeval informal units ("Estratos de Río del Oro"). This unit has been correlated to the distal Monte León Formation along the Atlantic coast that, together, record, the *Leonense* marine incursion of the *Patagonian Sea* at this latitude (Ameghino, 1906; Parras et al., 2008, 2012). The overlying Santa Cruz Formation marks the last phase of major sedimentation and fluvial deposition in the Patagonian Andes ca. 19-16 Ma, prior to regional surface uplift and incision of the foreland basin (Furque and Camacho, 1972; Bostelmann et al., 2013; Cuitiño et al., 2016).

DETRITAL U-Pb GEOCHRONOLOGY

Sampling and Analytical Methods

We collected twelve sandstone samples from the Paleocene – Miocene outcrop belt exposed near Cerro Castillo township, Chile, and Estancia Cancha Carrera, Argentina, townships in Patagonia (Fig. 1) from previously studied stratigraphic sections (Malumián and Caramés, 1997; Rodríguez Raising, 2010; Leonard, 2017). Sample information and locations are outlined in Table 1. Detrital zircons were extracted from ~5 kg medium-grained sandstone hand-samples using standard mineral separation techniques, including crushing and grinding, fractionation of magnetic minerals with a Frantz isodynamic magnetic separator, and settling through heavy liquids to exclude phases with densities less than 3.3 g/cm^3. Final zircon separates were mounted in epoxy resin together with fragments of the Sri Lanka standard zircon. The mounts were polished to a depth of ~20 μm, CL and BSE imaged, and cleaned prior to isotopic analysis. U-Pb geochronology of zircons was conducted by laser ablation multicollector inductively coupled plasma mass spectrometry (LA-MC-ICPMS) using a Photon Machines Analyte G2 excimer laser using a spot diameter of 30 μm at the Arizona LaserChron Center (Gehrels et al., 2008; Gehrels, 2011). Analytical methods and data are available in the Data Repository.

Preferred calculated U-Pb ages use the ^{204}Pb corrected ^{206}Pb/^{238}U ratio for <900 Ma grains and the ^{204}Pb corrected ^{206}Pb/^{207}Pb ratio for >900 Ma grains. Uncertainties shown in these tables are at the 1σ level, and include only measurement errors. Analyses that are >20% discordant and 5% reverse discordant (by comparison of ^{206}Pb/^{238}U and ^{206}Pb/^{207}Pb ages) were excluded from provenance interpretations and maximum depositional age interpretations. Pb*/U concordia diagrams (Fig. A1) and probability density plots (Figs. A2 and A3) were generated using the routines in Isoplot (Ludwig, 2008). The age-probability diagrams show each age and its uncertainty (for measurement error only) as a normal distribution, and sum all ages from a sample into a single curve. Probability density plots for individual samples are presented in Figures A2 and A3, and compiled formation-level datasets are shown in Figure 2. For samples that yielded youngest age groups that could represent conceivable maximum depositional ages, we calculated error-weighted mean ages based on the following criteria: age clusters contained at least two overlapping concordant grains at 2σ uncertainty (Fig. 3; Table 1). For published samples from the Punta Barrosa, Cerro Toro, Tres Pasos, and Dorotea Formations (Figs. 2 and 4), we recalculated relative probability density curves from published U-Pb geochronological data (Fildani et al., 2003; Romans et al., 2010; Fosdick et al., 2011, 2015; Bernhardt et al., 2012).

Results and Interpretations

Detrital zircon U-Pb geochronology results (1,579 dated grains) from the Cerro Castillo – Cancha Carrera area reveal distinctive age groups in variable proportions up-section (Fig. 2): (1) Cenozoic age clusters that include early Miocene-Oligocene (20-30 Ma), Eocene (33-45 Ma), and Paleocene (60-65 Ma) ages; (2) a range of Cretaceous ages with clusters at ca. 66-80 Ma, and 80-136 Ma (3) a Late Jurassic – earliest Cretaceous age group (136-175 Ma), (4) smaller proportions of Devonian-Permian ages (250-420 Ma), (5) early Paleozoic and Mesoproterozoic ages (420-1600 Ma), and (6) few Mesoproterozoic and older grains. Cenozoic and Cretaceous zircon grains are mostly large (>100 µm), euhedral to subhedral, magmatically zoned zircons. In contrast, Jurassic zircons are mostly small (<60 µm in width), subangular or broken fragments of long and narrow volcanic crystals. Paleozoic and Proterozoic grains are mostly small (<50 µm) subrounded to rounded grains.

Cerro Dorotea Formation

Detrital geochronology from four stratigraphic horizons (649 grains) within the mapped Cerro Dorotea Formation yields major age groups between 60-66 Ma, 74-115 Ma, 123-160 Ma, 473-630 Ma, 960-1130 Ma, and fewer early Paleozoic and Proterozoic zircons. The lowest sample (15LDC05) collected from the base of the formation yields an MDA of 65.8 ± 1.3 Ma. The middle samples (14AVDZ1 and 14AVDZ1), collected from thick trough cross-bedded tan and orangish brown sandstone with interbedded siltstone and coal-bearing mudstone, yield MDAs of 61.9 ± 0.3 Ma and 60.5 ± 0.8, respectively (Fig. 3). The stratigraphically highest level was sampled twice in the exact location, ~3 m below the top of the formation (14AVDZ3 + 15LDC02) yields a MDA of 60.2 ± 1.3 Ma.

Lower member of the Río Turbio Formation

Three samples (413 grains) collected from the overlying greenish gray and brown glauconitic sandstone units, interpreted as subaqueous deltaic deposits, yield similar zircon U-Pb age distributions with a pronounced Eocene peak, two Late Cretaceous age clusters, and few Jurassic ages (Fig. 2). Estimation of MDAs from the youngest zircon population indicates sedimentation of the basal glauconitic sandstone by ca. 47.1 ± 2.7 Ma (14LDC-DZ4) and the overlying brown deltaic sandstone unit by 46.3 ± 1.3 Ma (14LDC-DZ2). The uppermost sample collected from a glauconitic sandstone at the top of the exposed unit yields a youngest age cluster with a MDA of 41.3 ± 0.3 Ma (17CCRT2-29).

Upper member of the Río Turbio Formation

Three detrital zircon U-Pb geochronology samples (312 grains) from fossiliferous and highly bioturbated marine strata of the upper member of the Río Turbio Formation yield robust age populations between 29-45 Ma, 63-109, 113-137 Ma, 218-288 Ma, and few Late Jurassic grains (Fig. 2). Proterozoic grains are noticeably lacking compared to underlying detrital age distributions. Youngest age clusters from the bottom of the unit yield a MDA ca. 36.6 ± 0.3 Ma (RT28DZ08) and 35.4 ± 0.2 Ma (RT28DZ07). At the top of the ~230 m thick succession, organic-rich mudstones below the contact with the Río Guillermo Formation yield a MDA of ca. 26.6 ± 0.2 Ma (RT28DZ05).

Río Guillermo Formation

Two samples (205 grains) collected from the base of the Río Guillermo Formation yield U-Pb age peaks between 23-26 Ma, 33-36 Ma, a broad range of Mid to Late Cretaceous age between 72-128 Ma, 149-154 Ma, 275-304 Ma, and lesser numbers of Proterozoic grains (Fig.

2). The youngest zircon age peak from the bottom of the formation gives a MDA of ca. 24.3 ± 0.6 Ma (RT28DZ06). A second sample collected from the top of the Río Guillermo Formation, directly below a dated volcanic tuff (21.7 Ma zircon U-Pb SHRIMP-RG, Fosdick et al., 2011), yields a MDA of 22.8 ± 0.2 Ma (JCF09-237B).

The sampled section exhibits an upsection younging of zircons, increase in Cenozoic and Late Cretaceous zircons, and decrease in all zircon age groups older than ca. 135 Ma (Fig. 2). The most pronounced loss of Late Jurassic-Early Cretaceous (~20% to ~6%) and Paleozoic (40-17% to 7%), and Mesoproterozoic-Archean (20% to 8%) is observed across the Paleocene Cerro Dorotea Formation – middle Eocene Río Turbio Formation contact (Fig. 2 and Fig DZTREND). Only the Río Guillermo Formation exhibits a slight covarying increase in both the Late Jurassic-Early Cretaceous group and Paleozoic age group. These percentage trends persist, even when accounting for the large influx of Cenozoic grains, as shown by the normalized zircon age groups >66 Ma (Fig. 4).

DISCUSSION

Revised Timing of Foreland Sedimentation

New geochronological constraints on depositional ages in the Magallanes Basin suggest significantly younger timing for middle Cenozoic inland sea transgressions and onset of exclusively fluvial sedimentation in the study area (Fig. 5). These results redefine our understanding of the genetic relationship between sedimentation and changes in relative sea level, climate, and phases of deformation in the Andean orogenic belt (Fig. 6). Under the prevailing view, there are four major Cenozoic Atlantic transgressions in the Magallanes Basin of Patagonia and Tierra del Fuego: Maastrichtian-Danian, late Middle Eocene, Late Oligocene – Early Miocene (*Juliense*), and late Early Miocene (*Leonense*) (Fig. 6; Malumián and Náñez, 2011; Parras et al., 2012; Perkins et al., 2012). In the proximal Magallanes Basin near Cerro Castillo (Fig. 1), the Maastrichtian deltaic Dorotea Formation is overlain by the laterally discontinuous Paleocene Cerro Dorotea Formation and overlying Eocene estuarine and deltaic Río Turbio Formations (Fig. 5; Hünicken, 1955; Malumián and Caramés, 1997; Rodríguez Raising, 2010). Debate persists on the age of the Río Turbio Formation (Malumián and Caramés, 1997; Rodríguez Raising, 2010; Schweitzer et al., 2012), with early biostratigraphic studies reporting Eocene through Miocene (Riccardi and Rolleri, 1980) or exclusively Eocene biozones (Malumián and Caramés, 1997; Guerstein et al., 2014). Based on such age assignments for these strata, many workers have interpreted the upper Cerro Dorotea through Río Turbio deposits within the paleoclimatic context of Paleogene climatic optima such as the Paleocene-Eocene Thermal Maximum and Early Eocene Climatic Optimum (Fig. 6; e.g., Nullo and Combina, 2011). Our data support this age (65-60 Ma) and paleoclimatic interpretation for the Cerro Dorotea Formation through *only* the basal portion of the lower Río Turbio Formation, which is Lutetian (47-41 Ma) in age (Fig. 5). The Cerro Dorotea Formation is recognized in Argentina and assigned to the Danian mostly based on the foraminiferal content (Malumián and Náñez, 2011), but our radiometric age suggest a later, Selandian, maximum depositional age, giving the first formal confirmation of the occurrence of this Paleocene lithostratigraphic unit in Chile.

The subaqueous deltaic lower Río Turbio Formation contains detrital zircons that indicate Eocene sedimentation starting at ca. 47 Ma and continued through at least ca. 41 Ma (Fig. 5). These ages are compatible with Eocene leaf impressions, shark teeth, and marine invertebrate fossils recovered from these deposits (Griffin, 1991; Otero et al., 2013; Panti, 2016). Moreover, these strata show similar age, sedimentary facies, fossil content, and mineral composition to those of the Man Aike Formation near Lago Argentino (Casadío et al., 2009) and Sierra Baguales (Le Roux et al., 2010; Ugalde, 2014; Gutiérrez et al., 2017), pointing to stratigraphic correlation of a regional, renewed depositional phase of foreland sedimentation across the Paleocene unconformity surface.

In contrast, our findings from the upper Río Turbio Formation show substantially younger ages ca. 37-26 Ma (Fig. 5), indicating that these deposits are not associated with early/middle Eocene climatic events. Rather, they record latest Eocene through Oligocene paleoenvironmental and tectonic conditions (Fig. 6). These ages are notably younger than the ca. 46-39 Ma (Lutetian-Bartonian) dinocyst biostratigraphic ages from nearby sections in the Río Turbio Formation (Guerstein et al., 2014; González Estebenet et al., 2016), necessitating a potential revision to the chronostratigraphy in this area in light of our new radiometric data. The laterally discontinuous outcrops and lack of clear marker beds allow for the possibility that these sections are not chronostratigraphically equivalent with our sites. Poor microfaunal preservation within the Río Turbio Formation further challenges the comparison. We suggest that a latest Eocene through Oligocene age (this work) for the upper Río Turbio Formation is more compatible with paleobotanical data that suggest mesothermal conditions at high latitude, based on the abundance and diversity of fossilized *Nothofagus* morphotype leaf impressions and wood fragments (Hünicken, 1955). Whereas the warm early Eocene conditions in Patagonia favored high tropical (megathermal) plant diversity (Wilf et al., 2003; Panti, 2016), the Eocene-Oligocene transition ushered forth increased diversification of meso- and microthermal floral elements across southern Gondwana, including the widespread dominion of genus *Nothofagus* (Ortíz-Jaureguizar and Cladera, 2006; Acosta et al., 2014).

Our younger basin age model suggests that the deepening to offshore conditions in the upper Río Turbio Formation ca. 37 Ma coincides with basin subsidence and deepening observed in Tierra del Fuego concurrent with a late Eocene marine transgression (Fig. 6) and the beginning of the Antarctic ice sheet expansion (Zachos et al., 2001; Francis et al., 2008). Sustained shallow-marine conditions along the margin of the Magallanes Basin between ca. 37 and 26 Ma, despite Oligocene eustatic sea level fall suggests an additional tectonic mechanism for marine conditions. More broadly, we suggest that the upper Río Turbio Formation marks a phase of overall Oligocene basin deepening, eastward loading of the foreland, and diachronous marine flooding driven by topographic loading from the fold-and-thrust belt (Fosdick et al., 2011) and coeval transpression across the North Scotia Ridge (Lagabrielle et al., 2009) (Fig. 6). It follows that the marine *Juliense* deposits along the Atlantic coast (Parras et al., 2012) – and the subsurface marine sequence of the El Huemul Formation (Paredes et al., 2015) on the southern extreme of the San Jorge Basin – could record the diachronous distal record of tectonically driven basin flexure and marine flooding of Patagonia. Tectonic deepening in southern Patagonia is consistent with increases in Nd isotope ratios that suggest deepening episodes in the Drake Passage at 37 Ma and 34 Ma interpreted from increases in Nd isotope ratios (Livermore et al., 2007). However, relative sea level highs around Antarctica due to near-field processes during glaciation (e.g., Stocchi et al., 2013) may have also affected sea level in southeastern Patagonia prior to a global sea level decrease through the Oligocene.

New geochronological data from the overlying fluvial Río Guillermo Formation suggest its deposition took place between latest Chattian through Aquitanian time ca. 24-21 Ma (Fig. 5). These radiometric results revise the previously accepted biostratigraphic upper Eocene to lower Oligocene age (Malumián and Caramés, 1997; Vento et al., 2017) and the interpretation that the

Río Guillermo Formation predates a rejuvenated phase of Andean orogenesis. These coarse-grained strata reflect the first Cenozoic fully continental conditions on the Patagonian foreland in the area. The onset of fluvial deposition coincides with ca. 27-21 Ma fault motion on the Río El Ríncon-Castillo thrusts (Fosdick et al., 2011), suggesting these deposits reflect increased supply of tectonically generated sediment (c.f., Armitage et al., 2011) during structural uplift and unroofing of the Patagonian orogen. This interpretation is consistent with published subsurface data just to the south of our study area (Fig. 1) that record latest Eocene through early Miocene prograding clastic strata south of our study area (Gallardo, 2015).

REORGANIZATION OF SEDIMENT PROVENANCE AND ROUTING

Detrital provenance data from the Upper Cretaceous – Miocene basin infill track changes in relative proportions of zircon age groups for pre-Cenozoic age groups (Fig. 2). A comparison with the Upper Cretaceous basin record and our new data show the upsection rise and subsequent loss of Jurassic – Early Cretaceous (J-K1) grains (blue wedge), a progressive loss of Precambrian and Paleozoic grains (browns and pink wedges), and an overall increase in Late Cretaceous and Cenozoic igneous sources (gray and white wedges). Notably, the Paleocene Cerro Dorotea Formation maintains similar provenance and gross depositional character to the underlying Dorotea Formation. This similarity indicates little to no drainage divide reorganization nor exposure of new sources during southward building of the continental shelf (Schwartz and Graham, 2015a) from Maastrichtian to earliest Cenozoic time. Moreover, this observation is noteworthy because of the discontinuous nature of the Cerro Dorotea Formation along the frontal monocline, which has invited debate regarding its original lateral extent and subsequent erosion versus heterogeneous depositional footprint (e.g., Fosdick et al., 2015). The Paleocene foreland basin phase along this sector of the basin may have once been more geographically widespread prior to erosional removal and resumed deposition with the middle Eocene Río Turbio Formation that forms the Paleogene unconformity (Fig. 6).

The largest shift in sediment provenance signature occurred across the Paleocene Cerro Dorotea and the middle Eocene Río Turbio Formation boundary, marked by a conspicuous decline of Late Jurassic and Paleozoic zircons (Figs. 2 and 4). Zircons of these ages are sourced from hinterland thrust sheets (Fig. 1) that expose the Upper Jurassic volcanic Tobífera Formation (Pankhurst et al., 2000; Calderón et al., 2007) and Paleozoic basement (Hervé et al., 2003; Lacassie et al., 2006; Pankhurst et al., 2006). The concurrent increase in Cenozoic zircons from the Patagonian Batholith may act to swamp out the signal from these older zircon sources. However, a comparison of relative proportion of pre-66 Ma age groups show similar trends in the rise and decline of the Jurassic and Paleozoic age groups (Fig. 4). We interpret this initial shift as likely a consequence of tectonic changes in sediment routing between ca. 60 and 44 Ma, when the basin became topographically isolated from northwestern hinterland sources during deformation and widening across the external thrust-belt.

Our age control of the Paleogene unconformity improves upon the work of Fosdick et al. (2015) who compared provenance and burial histories of the Dorotea Formation with the upper Río Turbio Formation, but lacked higher provenance resolution from intervening deposits. Evidence of coeval basin burial thermal heating (Fosdick et al., 2015; Süssenberger et al., 2017) in the central thrust belt and development of a basin-wide foreland unconformity is consistent with this timeframe. New provenance data sheds light on the timing of Tenerife thrusting (Fig. 6) and further supports an Eocene phase of orogenesis that is well-documented in the Fuegian

Andes (Barbeau et al., 2009), but remains enigmatic in the Southern Patagonian Andes. This finding suggests that, rather than being an inactive foreland basin during this time (Sachse et al., 2015; Horton and Fuentes, 2016), a more continuous fold-thrust belt and basin depocenter connected the Patagonian and Fuegian Andes during development of the Fuegian orocline (Ghiglione et al., 2010).

These upsection trends continue into Oligocene time when sediment provenance of the upper Río Turbio Formation reflects predominantly Cretaceous and younger age peaks. Prominent Eocene and Late Cretaceous age clusters include two new populations – denoted here as K4 (ca. 80-66 Ma) and P2 (ca. 20-35 Ma) – that are not recognized in batholith geochronology datasets (Hervé et al., 2007) and extend the record of pulsed activity of arc magmatism (Fig. 2). By ca. 26 Ma and the end of the marine sedimentation at this latitude, detrital zircons derived from the Late Jurassic Tobífera thrust sheets (Fig. 1), which were once a dominant sediment source to the Cenomanian-Paleocene basin, are virtually absent in the basin fill. Synchronous with this change in depositional environment is a marked provenance shift to increased mafic volcanic and recycled sedimentary sources, suggesting the change in environment is linked to upland tectonic/climate changes with a lesser control from low-stand in global sea level (Leonard, 2017). This timing of transition to fully continental sedimentation coincides with deformation in the fold-and-thrust belt at Río El Ríncon thrust and related structures (Fosdick et al., 2011). We suggest the Río Guillermo Formation represents tectonically generated sediment (e.g., Horton et al., 2004; Armitage et al., 2011) associated with this phase of deformation.

Fluvial sedimentation was temporarily disrupted by flooding of the foreland basin by the *Leonense* marine incursion (Ameghino, 1906; Parras et al., 2012; Cuitiño et al., 2012), which may have been further enhanced by subsidence loading during Toro thrust faulting (Fig. 6). Resumed fluvial deposition of the Santa Cruz Formation is classically cited as the molasse deposits of the main phase of Miocene Andean orogenesis and surface uplift (e.g., Blisniuk et al., 2005; Ramos, 2005; Bostelmann et al., 2013; Cuitiño et al., 2016), Published detrital geochronology from the overlying middle Miocene Santa Cruz Formation yields dominantly (>70%) Late Cretaceous zircons (Fosdick et al., 2015). Based on modeling of detrital zircon U-Pb-He thermochronological data, Fosdick et al. (2015) suggested these grains were recycled from the Upper Cretaceous clastic wedge rather than direct sourcing of the Mesozoic batholith. Our data from underlying strata corroborate this interpretation and capture a more complete transition of provenance loss of the Jurassic and Paleozoic age groups.

General provenance and sediment recycling

The rise and subsequent isolation of diagnostic sediment sources or detrital zircon age groups bears on resolving complexities from sediment recycling (Schmitt and Steidtmann, 1990; Dickinson et al., 2009) and variability in zircon fertility (Moecher and Samson, 2006). As such, a geologically diagnostic age source – especially one with smaller and/or more fragile grains (e.g., volcanics) – is a useful tracer for identifying primary versus recycled sources and constraints on movement of orogenic drainage divides during changes in orogenic wedge behavior. The Eocene-through Oligocene upsection depletion of Jurassic and Paleozoic sources near 51°S, concurrent with sustained dominance of plutonic arc-derived Cretaceous zircons (Fig. 4), suggests recycling of the Cretaceous strata in the Río Turbio Formation and winnowing of the smaller and more fragile Jurassic volcanic and Paleozoic zircons during sediment transport. Moreover, the isolation of hinterland and primary Cretaceous batholith sources requires a cratonward shift in the drainage divide by ca. 44 Ma. This change in sediment routing was followed by subsequent hinterland shift some time after ca. 18 Ma deposition of the final foreland basin phase of sedimentation and development of the Chile Ridge slab window beneath Patagonia (Fig. 6). Today, the hinterland high peaks constitute the Patagonian Andes drainage divide; upland sources to rivers (Pepper et al., 2016) and glacial valleys drain both sides of the Andes and Tobífera thrusts (Fig. 1).

SUMMARY AND IMPLICATIONS

In summary, new estimates of maximum depositional ages from detrital geochronology data require a revised chronostratigraphy of the middle Cenozoic strata. Our study confirms a Selandian maximum depositional age for the Cerro Dorotea Formation, previously constrained by biostratigraphy to the Danian. Sediment provenance data from the Cenozoic Magallanes Basin at 51°S track the decline of once prominent hinterland sources between ca. 60-44 Ma. We suggest a major change in sediment routing and paleogeography during this time that we attribute to a phase of Eocene orogenesis and uplift of a topographic barrier that isolated the basin from Paleozoic and Late Jurassic-Early Cretaceous sources (Fig. 6). We also identify a previously unrecognized early Oligocene period of marine deposition from ca. 36 to 26 Ma in the proximal foredeep depozone (upper Río Turbio Formation), followed by a major change to nonmarine sedimentation ca. 24 Ma. Here, we propose that the upper Río Turbio and Río Guillermo Formations, together, reflect a genetically linked stratigraphic pair that show early Oligocene basin deepening and subsequent latest Oligocene – Early Miocene deposition of coarse-grained sediments derived from the Patagonian hinterland (Fig. 6).

Moreover, an eastward incursion of an embayed foredeep trough may link the upper Río Turbio Formation to the distal San Julián, suggesting a tectonic loading origin for the *Juliense* phase of the Patagonian Sea. Additional stratigraphic correlation to the Atlantic margin is needed to test this hypothesis. The late Oligocene – early Miocene synchronicity of (1) proximal fluvial facies (Río Guillermo Formation) and distal marine facies (*Juliense* and *Leonense*), (2) active orogenic deformation (Río El Rincon and Toro thrust faults), and (3) sustained global sea level highstand, taken together, indicates high sediment supply during shortening of the thrust-belt (Fig. 6). In the case of the Oligocene – middle Miocene Patagonian record, we suggest that the combined effects of tectonics – flexural loading of the upper plate and increased sediment supply from actively exhuming orogenic sources – are primary drivers for marine transgressions.

Rejuvenated Late Oligocene through middle Miocene retroarc foreland sedimentation in southern Patagonia – and elsewhere along the Andean margin (e.g., Carrapa et al., 2005; Perez and Horton, 2014; Horton and Fuentes, 2016; Fosdick et al., 2017) – may signal a Cordilleran-scale upper plate transition to a dominantly compressional margin and active retroarc foreland basin systems (Horton, 2018; Chen et al., 2019) that include the southern Patagonian Andes sector. This response was likely due to increased plate convergence (Somoza and Ghidella, 2012) and initiation of the Nazca plate subduction regime (e.g., Barckhausen et al., 2008). In Patagonia, regional retroarc deformation and basin development may have been enhanced by three-dimensional stress from transpressional tectonics along the North Scotia Ridge (Bry et al., 2004; Ramos and Ghiglione, 2008; Lagabrielle et al., 2009). These findings underscore central requirements of detailed chronology and provenance to develop basin age models and understanding of long-term changes in sources that reflect orogen-scale responses to tectonics, climate, and eustasy.

ACKNOWLEDGMENTS

Research was supported by the U.S. National Science Foundation Award EAR-1649585 to JCF, the Robert R. Shrock Foundation at Indiana University, and Project Anillo de Investigación en Ciencia Antártica (ATC-105). T. Schwartz, S. Casadío, and A. Parras contributed to discussions on Patagonian geology. La Cumbre Baguales Geo-Paleontological Park, Hotel Remota, the Torres del Paine Municipality, Hielos Patagónicos and Mountain Travel, at Puerto Natales, and N. Raffer provided logistical support. We thank S.F Alvarez for permission to conduct fieldwork at the Estancia Cancha Carrera. The Arizona LaserChron Center (NSF Award EAR-1338583) provided expert analytical assistance. Reviews on a previous version of the manuscript by David Barbeau, George Dix, Nicholas Perez, and Andrea Stevens Goddard improved the scope and clarity of the work.

REFERENCES CITED

Acosta, M.C., Mathiasen, P., and Premoli, A.C., 2014, Retracing the evolutionary history of Nothofagus in its geo-climatic context: New developments in the emerging field of phylogeology: Geobiology, v. 12, p. 497–510, doi:10.1111/gbi.12098.

Ameghino, F., 1906, Les formations sédimentaires du Crétacé Supérieur et du Tertiaire de Patagonie avec un parallelé entre leurs faunes mammalogiques et celles de l´ancien continent.: Anales del Museo Nacional de Buenos Aires (tercera serie), v. 8, p. 1–568.

Armitage, J.J., Duller, R.A., Whittaker, A.C., and Allen, P.A., 2011, Transformation of tectonic and climatic signals from source to sedimentary archive: Nature Geoscience, v. 4, p. 231–235, doi:10.1038/ngeo1087.

Barbeau, D.L., Olivero, E.B., Swanson-Hysell, N.L., Zahid, K.M., Murray, K.E., and Gehrels, G.E., 2009, Detrital-zircon geochronology of the eastern Magallanes foreland basin: Implications for Eocene kinematics of the northern Scotia Arc and Drake Passage: Earth and Planetary Science Letters, v. 284, p. 489–503, doi:10.1016/j.epsl.2009.05.014.

Barckhausen, U., Ranero, C.R., Cande, S.C., Engels, M., and Weinrebe, W., 2008, Birth of an intraoceanic spreading center: Geology, v. 36, p. 767–770.

Beaumont, C., Fullsack, P., and Hamilton, J., 1992, Erosional control of active compressional orogens, *in* McClay, K.R. ed., Thrust Tectonics, Chapman and Hall, p. 1–18.

Bernhardt, A., Jobe, Z.R., Grove, M., and Lowe, D.R., 2012, Palaeogeography and diachronous infill of an ancient deep-marine foreland basin, Upper Cretaceous Cerro Toro Formation, Magallanes Basin: Basin Research, v. 24, p. 269–294, doi:10.1111/j.1365-2117.2011.00528.x.

Biddle, K.T., Uliana, M.A., Mitchum, R.M., Fitzgerald, M.G., and Wright, R.C., 1986, The stratigraphic and structural evolution of the central and eastern Magallanes Basin, southern South America, *in* Allen, P.A. and Homewood, P. eds., Foreland Basins, Oxford, UK, Blackwell Publishing Ltd., v. 8, p. 41–61, doi:doi: 10.1002/9781444303810.ch2.

Blisniuk, P.M., Stern, L.A., Chamberlain, C.P., Idleman, B., and Zeitler, P.K., 2005, Climatic and ecologic changes during Miocene surface uplift in the Southern Patagonian Andes: Earth and Planetary Science Letters, v. 230, p. 125–142, doi:10.1016/j.epsl.2004.11.015.

Bonnet, S., and Crave, A., 2003, Landscape response to climate change: Insights from experimental modeling and implications for tectonic versus climatic uplift of topography: Geology, v. 31, p. 123–126, doi:10.1130/0091-7613(2003)031<0123:LRTCCI>2.0.CO.

Bostelmann, J.E. et al., 2013, Burdigalian deposits of the Santa Cruz Formation in the Sierra Baguales, Austral (Magallanes) Basin: Age, depositional environment and vertebrate fossils: Andean Geology, v. 40, p. 458–489, doi:10.5027/andgeoV40n3-a04.

Browning, J. V., Miller, K.G., McLaughlin, P.P., Kominz, M.A., Sugarman, P.J., Monteverde, D., Feigenson, M.D., Hern??ndez, J.C., and Hernández, J.C., 2006, Quantification of the effects of eustasy, subsidence, and sediment supply on Miocene sequences, mid-Atlantic margin of the United States: Bulletin of the Geological Society of America, v. 118, p. 567–588, doi:10.1130/B25551.1.

Bry, M., White, N., Singh, S., England, R., and Trowell, C., 2004, Anatomy and formation of oblique continental collision: South Falkland basin: Tectonics, v. 23, p. 1–20, doi:10.1029/2002TC001482.

Calderón, M., Fildani, A., Hervé, F., Fanning, C.M., Weislogel, A., and Cordani, U., 2007, Late Jurassic bimodal magmatism in the northern sea-floor remnant of the Rocas Verdes basin, southern Patagonian Andes: Journal of the Geological Society, London, v. 164, p. 1011–1022.

Carrapa, B., Adelmann, D., Hilley, G.E., Mortimer, E., Sobel, E.R., and Strecker, M.R., 2005, Oligocene range uplift and development of plateau morphology in the southern central Andes: Tectonics, v. 24, p. 1–19, doi:10.1029/2004TC001762.

Casadío, S., Griffin, M., Marenssi, S., Net, L., Parras, A., Raising, M.R., and Santillana, S., 2009, Paleontology and sedimentology of Middle Eocene rocks in Lago Argentino area, Santa Cruz Province, Argentina: Ameghiniana, v. 46, p. 27–47.

Chen, Y.-W., Wu, J., and Suppe, J., 2019, Southward propagation of Nazca subduction along the Andes: Nature, v. 565, p. 441–447, doi:10.1038/s41586-018-0860-1.

Christie-blick, N., 1991, Onlap, offlap, and the origin of unconformity-bounded depositional sequences: Marine Geology, v. 97, p. 35–56.

Clift, P.D., Shimizu, N., D, L.G., Blusztaign, J.S., Gaedicke, C., Schluter, H.-H., Clark, M.K., and Amjad, S., 2001, Development of the Indus Fan and its significance for the erosional history development of the Indus Fan and its significance for the erosional history of the Western Himalaya and Karakoram: Geological Society of America Bulletin, v. 113, p. 1039–1051, doi:10.1130/0016-7606(2001)113<1039.

Cox, R., Lowe, D.R., and Cullers, R.L., 1995, The influence of sediment recycling and basement composition on evolution of mudrock chemistry in the southwestern United States: Geochimica et Cosmochimica Acta, v. 59, p. 2919–2940, doi:10.1016/0016-7037(95)00185-9.

Cruz, L., Malinski, J., Hernandez, M., Take, a., and Hilley, G.E., 2011, Erosional control of the kinematics of the Aconcagua fold-and-thrust belt from numerical simulations and physical experiments: Geology, v. 39, p. 439–442, doi:10.1130/G31675.1.

Cuitiño, J.I., Fernicola, J.C., Kohn, M.J., Trayler, R., Naipauer, M., Bargo, M.S., Kay, R.F., and Vizcaíno, S.F., 2016, U-Pb geochronology of the Santa Cruz Formation (early Miocene) at the Río Bote and Río Santa Cruz (southernmost Patagonia, Argentina): Implications for the correlation of fossil vertebrate localities: Journal of South American Earth Sciences, v. 70, p. 198–210, doi:10.1016/j.jsames.2016.05.007.

Cuitiño, J.I., Pimentel, M.M., Ventura Santos, R., and Scasso, R. a., 2012, High resolution isotopic ages for the early Miocene “Patagoniense” transgression in Southwest Patagonia: Stratigraphic implications: Journal of South American Earth Sciences, v. 38, p. 110–122, doi:10.1016/j.jsames.2012.06.008.

Cuitiño, J.I., and Scasso, R.A., 2010, Sedimentología y paleoambientes del Patagoniano y su transición a la Formatión Santa Cruz al sur del Lago Argentino, Patagonia Austral: Revista de la Asociación Geológica Argentina, v. 66, p. 406–417.

Dahlen, F. a., Suppe, J., and Davis, D., 1984, Mechanics of fold-and-thrust belts and accretionary wedges Cohesive Coulomb theory: Journal of Geophysical Research, v. 89, p. 10087–10101, doi:10.1029/JB089iB12p10087.

Dickinson, W.R., Lawton, T.F., and Gehrels, G.E., 2009, Recycling detrital zircons: A case study from the Cretaceous Bisbee Group of southern Arizona: Geology, v. 37, p. 503–506, doi:10.1130/G25646A.1.

Dix, G.R., and Parras, A., 2014, Integrated diagenetic and sequence stratigraphy of a late Oligocene-early Miocene, mixed-sediment platform (Austral Basin, southern Patagonia): Resolving base-level and paleoceanographic changes, and paleoaquifer characteristics: Sedimentary Geology, v. 307, p. 17–33, http://dx.doi.org/10.1016/j.sedgeo.2014.04.003.

Eronen, J.T., Janis, C.M., Chamberlain, C.P., and Mulch, A., 2015, Mountain uplift explains differences in Palaeogene patterns of mammalian evolution and extinction between North America and Europe:

Fildani, A., Cope, T.D., Graham, S.A., and Wooden, J.L., 2003, Initiation of the Magallanes foreland basin: Timing of the southernmost Patagonian Andes orogeny revised by detrital zircon provenance analysis: Geology, v. 31, p. 1081–1084.

Flemings, P.B., and Jordan, T.E., 1989, A synthetic stratigraphic model of foreland basin development: Journal of Geophysical Research, v. 94, p. 3851–3866.

Fosdick, J.C., Graham, S.A., and Hilley, G.E., 2014, Influence of attenuated lithosphere and sediment loading on flexure of the deep-water Magallanes retroarc foreland basin, Southern Andes: Tectonics, v. 33, p. 2505–2525, doi:10.1002/2014TC003684.

Fosdick, J.C., Grove, M., Graham, S.A., Hourigan, J.K., Lovera, O., and Romans, B.W., 2015, Detrital thermochronologic record of foreland burial heating, sedimentary provenance, and orogenesis in Patagonia: Basin Research, v. 27, p. 546–572, doi:10.1111/bre.12088.

Fosdick, J.C.C., Reat, E.J.J., Carrapa, B., Ortíz, G., Alvarado, P.M.M., Ortiz, G., and Alvarado, P.M.M., 2017, Retroarc basin reorganization and aridification during Paleogene uplift of the southern central Andes: Tectonics, v. 36, p. 493–514, doi:10.1002/2016TC004400.

Fosdick, J.C., Romans, B.W., Fildani, A., Bernhardt, A., Calderón, M., and Graham, S. a., 2011, Kinematic evolution of the Patagonian retroarc fold-and-thrust belt and Magallanes foreland basin, Chile and Argentina, 51°30'S: Geological Society of America Bulletin, v. 123, p. 1679–1698, http://gsabulletin.gsapubs.org/cgi/doi/10.1130/B30242.1 (accessed August 2011).

Francis, J.E. et al., 2008, Chapter 8 From Greenhouse to Icehouse - The Eocene/Oligocene in Antarctica: Developments in Earth and Environmental Sciences, v. 8, p. 309–368, doi:10.1016/S1571-9197(08)00008-6.

Furque, G., and Camacho, H.H., 1972, El Cretácico Superior y Terciario de la región Austral del Lago Argentino (Provincia de Santa Cruz). In Jornadas Geológicas Argentinas, No. 4, Actas 3: 61-76. Buenos Aires.No Title: Jornadas Geológicas Argentinas, v. 4, p. 61–76.

Galeazzi, J.S., 1998, Structural and stratigraphic evolution of the western Malvinas Basin, Argentina: American Association of Petroleum Geologists Bulletin, v. 82, p. 596–636, doi:10.1306/1D9BC5C5-172D-11D7-8645000102C1865D.

Gallardo, R.E., 2015, Seismic sequence stratigraphy of a foreland unit in the Magallanes-Austral Basin, Dorado Riquelme Block, Chile: Implications for deep-marine reservoirs: Latin American Journal of Sedimentology and Basin Analysis, v. 21, p. 49–64.

Gehrels, G., 2011, Detrital Zircon U-Pb Geochronology: Current Methods and New Opportunities: Tectonics of Sedimentary Basins, p. 45–62, doi:10.1002/9781444347166.ch2.

Gehrels, G.E., Valencia, V.A., and Ruiz, J., 2008, Enhanced precision, accuracy, efficiency, and spatial resolution of U-Pb ages by laser ablation-multicollector-inductively coupled plasma-mass spectrometry: Geochemistry, Geophysics, Geosystems, v. 9, p. 1–13, doi:10.1029/2007GC001805.

George, S.W.M., Davis, S.N., Fernández, R.A., Manríquez, L.M.E., Leppe, M.A., Horton, B.K., and Clarke, J.A., 2019, Chronology of deposition and unconformity development across the Cretaceous–Paleogene boundary, Magallanes-Austral Basin, Patagonian Andes: Journal of South American Earth Sciences, p. 102237, doi:10.1016/j.jsames.2019.102237.

Ghiglione, M.C., Quinteros, J., Yagupsky, D., Bonillo-Martínez, P., Hlebszevtich, J., Ramos, V. a., Vergani, G., Figueroa, D., Quesada, S., and Zapata, Y.T., 2010, Structure and tectonic history of the foreland basins of southernmost South America: Journal of South American Earth Sciences, v. 29, p. 262–277, doi:10.1016/j.jsames.2009.07.006.

Ghiglione, M.C., Ramos, V., Cuitiño, J., and Barberón, V., 2016, Growth of the Southern Patagonian Andes (46–53°S) and its relation with subduction processes, *in* Folguera, A., Naipauer, M., Sagripanti, L., Ghiglione, M.C., Orts, D.L., and Giambiagi, L. eds., Growth of the Southern Andes, Berlin, Springer, p. 201–240.

González, E., 2015, Estratigrafía secuencial y sedimentología de la Formación Dorotea (Maastrichtiano), sector Río de las Chinas, Región de Magallanes y Antártica Chilena, Chile (50°S), Undergraduate thesis: Universidad de Chile, 153 p.

González Estebenet, M.S., Guerstein, G.R., Rodríguez Raising, M.E., Ponce, J.J., and Alperín, M.I., 2016, Dinoflagellate cyst zonation for the middle to upper Eocene in the Austral Basin, southwestern Atlantic Ocean: implications for regional and global correlation: Geological Magazine, v. 154, p. 1022–1036.

Griffin, M., 1991, Bivalves From the Rio Turbio Formation, Eocene Southwestern Patagonia (Argentina): Journal of Paleontology, v. 65, p. 119–146.

Guerstein, G.R., González Estebenet, M.S., Alperín, M.I., Casadío, S.A., and Archangelsky, S., 2014, Correlation and paleoenvironments of middle Paleogene marine beds based on dinoflagellate cysts in southwestern Patagonia, Argentina: Journal of South American Earth Sciences, v. 52, p. 166–178, doi:10.1016/j.jsames.2014.02.011.

Gutiérrez, N.M., Le Roux, J.P., Vásquez, A., Carreño, C., Pedroza, V., Araos, J., Oyarzún, J.L., Pino, J.P., Rivera, H.A., and Hinojosa, L.F., 2017, Tectonophysics Tectonic events reflected by palaeocurrents, zircon geochronology, and palaeobotany in the Sierra Baguales of Chilean Patagonia: Tectonophysics, v. 695, p. 76–99, doi:10.1016/j.tecto.2016.12.014.

Hervé, F., Fanning, C.M., and Pankhurst, R.J., 2003, Detrital zircon age patterns and provenance of the metamorphic complexes of southern Chile: Journal of South American Earth Sciences, v. 16, p. 107–123, doi:10.1016/S0895-9811(03)00022-1.

Horton, B.K., 2018, Sedimentary record of Andean mountain building: Earth-Science Reviews, v. 178, p. 279–309, doi:10.1016/j.earscirev.2017.11.025.

Horton, B.K., Constenius, K.N., and DeCelles, P.G., 2004a, Tectonic control on coarse-grained foreland-basin sequences: An example from the Cordilleran foreland basin, Utah: Geology, v. 32, p. 637, doi:10.1130/G20407.1.

Horton, B.K., Constenius, K.N., and DeCelles, P.G., 2004b, Tectonic control on coarse-grained foreland-basin sequences: An example from the Cordilleran foreland basin, Utah: Geology, v. 32, p. 637–640, doi:10.1130/G20407.1.

Horton, B.K., and Fuentes, F., 2016, Sedimentary record of plate coupling and decoupling during growth of the Andes: Geology, v. 44, p. 647–650, doi:10.1130/G37918.1.

Houben, A.J.P. et al., 2013, Reorganization of Southern Ocean: Science, v. 340, p. 341–344.

Houston, W.S., Huntoon, J.E., and Kamola, D.L., 2000, Modeling of cretaceous foreland-basin parasequences, Utah, with implications for timing of Sevier thrusting: Geology, v. 28, p. 267–270.

Hünicken, M.A., 1955, Depósitos Neocretácicos y Terciarios del extremo SSW de Santa Cruz (Cuenca Carbonífera de Río Turbio): Revista del Instituto Nacional de Investigaciones en Ciencias Naturales, Ciencias Geológicas, v. 4, p. 1–161.

Johnsson, M.J., and Basu, A., 1993, Processes Controlling the Composition of Clastic Sediments: Geological Society of America Special Paper, v. 284.

Jordan, T.E., Allmendinger, R.W., Damanti, J.F., and Drake, R.E., 1993, Chronology of Motion in a Complete Thrust Belt: The Precordillera, 30-31°S, Andes Mountains: Journal of Geology, v. 101, p. 135–156, doi:10.1086/648213.

Lacassie, J.P., Hervé, F., and Roser, B., 2006, Sedimentary provenance study of the post-Early Permian to pre-Early Cretaceous metasedimentary Duque de York Complex, Chile: Revista Geologica de Chile, v. 33, p. 199–219.

Lagabrielle, Y., Goddéris, Y., Donnadieu, Y., Malavieille, J., and Suarez, M., 2009, The tectonic history of Drake Passage and its possible impacts on global climate: Earth and Planetary Science Letters, v. 279, p. 197–211, doi:10.1016/j.epsl.2008.12.037.

Leonard, J.S., 2017, Miocene growth of the Patagonian Andes revealed by sedimentary provenance of the Río Guillermo Formation, Magallanes-Austral Basin, Chile and Argentina (51°30’S): M.S. Thesis, Indiana University, 55 p.

Limonta, M., Garzanti, E., Resentini, A., Ando, S., Boni, M., and Bechstadt, T., 2015, Multicyclic sediment transfer along and across convergent plate boundaries (Barbados, Lesser Antilles): Basin Research, v. 27, p. 696–713, doi:10.1111/bre.12095.

Ludwig, K.R., 2008, User’s Manual for Isoplot 3.60 - A Geochronological Toolkit for Microsoft Excel: Berkeley Geochronology Center Special Publication, v. 4, p. 77.

Macellari, C.E., Barrio, C.A., and Manassero, M.J., 1989, Upper Cretaceous to Paleocene depositional sequences and standstone petrography of southwestern Patagonia (Argentina and Chile): Journal of South American Earth Sciences, v. 2, p. 223–239.

Malkowski, M.A., Sharman, G.R., Schwartz, T.M., and Graham, S.A., 2013, Spatial variations in deposional setting during foreland basin initiation, Magallanes-Austral basin, Patagonia: linking ancient deep-water lobes to their shelfal source, *in* Stanford Project on Deepwater Depositional Systems Consortium Report, p. 43.

Malumián, N., and Caramés, A., 1997, Upper Campanian-Paleogene from the Río Turbio coal measures in southern Argentina: micropaleontology and the Paleocene/Eocene boundary: Journal of South American Earth Sciences, v. 10, p. 189–201.

Malumián, N., and Náñez, C., 2011, The Late Cretaceous-Cenozoic transgressions in Patagonia and the Fuegian Andes: Foraminifera, palaeoecology, and palaeogeography: Biological Journal of the Linnean Society, v. 103, p. 269–288, doi:10.1111/j.1095-8312.2011.01649.x.

Malumián, N., Panza, J.L., Parisi, C., Naňez, C., Caramés, A., and Torre, A., 2000, Hoja Geológica 5172-III, Yacimiento Río Turbio (1:250,000): Servicio Geológico Minero Argentino, Boletin, v. 247, p. 180.

Manríquez, L.M.E., Lavina, E.L.C., Fernández, R.A., Trevisan, C., and Leppe, M.A., 2019, Journal of South American Earth Sciences Campanian-Maastrichtian and Eocene stratigraphic architecture , facies analysis , and paleoenvironmental evolution of the northern Magallanes Basin (Chilean Patagonia): Journal of South American Earth Sciences, v. 93, p. 102–118, doi:10.1016/j.jsames.2019.04.010.

Marshall, L.G., Webb, S.D., Sepkoski, J.J., and Raup, D.M., 1982, Mammalian Evolution and the Great American Interchange Published: Science, v. 215, p. 1351–1357.

Miller, K.G., 2008, Sea level change, last 250 million years, *in* Encyclopedia of Paleoclimatology and Ancient Environments, p. 879–887.

Miller, K.G., Kominz, M. a, Browning, J. V, Wright, J.D., Mountain, G.S., Katz, M.E., Sugarman, P.J., Cramer, B.S., Christie-Blick, N., and Pekar, S.F., 2005, The Phanerozoic record of global sea-level change.: Science, v. 310, p. 1293–1298.

Moecher, D.P., and Samson, S.D., 2006, Differential zircon fertility of source terranes and natural bias in the detrital zircon record: Implications for sedimentary provenance analysis: Earth and Planetary Science Letters, v. 247, p. 252–266, doi:10.1016/j.epsl.2006.04.035.

Natland, M.L., Gonzales, E.P., Cañon, A., and Ernst, M., 1974, A system of stages for correlation of Magallanes Basin sediments: Geological Society of America, Memoir, v. 139, p. 1–73.

Nie, J., Horton, B.K., Saylor, J.E., Mora, A.A., Mange, M., Garzione, C.N., Basu, A., Moreno, C.J., Caballero, V., and Parra, M., 2012, Integrated provenance analysis of a convergent retroarc foreland system: U-Pb ages, heavy minerals, Nd isotopes, and sandstone compositions of the Middle Magdalena Valley basin, northern Andes, Colombia: Earth-Science Reviews, v. 110, p. 111–126, doi:10.1016/j.earscirev.2011.11.002.

Nullo, F., and Combina, A., 2011, Patagonian continental deposits (Cretaceous-Tertiary):

Biological Journal of the Linnean Society, v. 103, p. 289–304, doi:10.1111/j.1095-8312.2011.01654.x.

Olivero, E.B., and Malumián, N., 2008, Mesozoic-Cenozoic stratigraphy of the Fuegian Andes, Argentina: Geologica Acta, v. 6, p. 5–18, doi:10.1344/105.

Ortíz-Jaureguizar, E., and Cladera, G.A., 2006, Paleoenvironmental evolution of southern South America during the Cenozoic: Journal of Arid Environments, v. 66, p. 498–532, doi:10.1016/j.jaridenv.2006.01.007.

Otero, R.A., Oyarzún, J.L., Soto-Acuña, S., Yury-Yáñez, R.E., Gutierrez, N.M., Le Roux, J.P., Torres, T., and Hervé, F., 2013, Neoselachians and Chimaeriformes (Chondrichthyes) from the latest Cretaceous-Paleogene of Sierra Baguales, southernmost Chile. chronostratigraphic, paleobiogeographic and paleoenvironmental implications: Journal of South American Earth Sciences, v. 48, p. 13–30.

Otero, R. a., Torres, T., Roux, J.P. Le, Hervé, F., Fanning, C.M., Yury-Yáñez, R.E., and Rubilar-rogers, D., 2012, A Late Eocene age proposal for the Loreto Formation (Brunswick Peninsula, southernmost Chile), based on fossil cartilaginous fishes, paleobotany and radiometric evidence: Andean Geology, v. 39, p. 180–200.

Painter, C.S., and Carrapa, B., 2013, Flexural versus dynamic processes of subsidence in the North American Cordillera foreland basin: Geophysical Research Letters, v. 40, p. 4249–4253, doi:10.1002/grl.50831.

Palazzesi, L., Barreda, V.D., Cuitiño, J.I., Guler, M. V., Tellería, M.C., and Ventura Santos, R., 2014, Fossil pollen records indicate that Patagonian desertification was not solely a consequence of Andean uplift: Nature Communications, v. 5, p. 3558, doi:10.1038/ncomms4558.

Pankhurst, R.J., Rapela, C.W., Fanning, C.M., and Márquez, M., 2006, Gondwanide continental collision and the origin of Patagonia: Earth-Science Reviews, v. 76, p. 235–257, doi:10.1016/j.earscirev.2006.02.001.

Pankhurst, R.J., Riley, T.R., Fanning, C.M., and Kelley, S.P., 2000, Episodic silicic volcanism in Patagonia and the Antarctic Peninsula: Chronology of magmatism associated with the break-up of Gondwana: Journal of Petrology, v. 41, p. 605–625.

Panti, C., 2016, Myrtaceae fossil leaves from the Río Turbio Formation (Middle Eocene), Santa Cruz Province, Argentina: Historical Biology, v. 28, p. 459–469.

Paredes, J.M., Foix, N., Guerstein, G.R., Guler, M. V., Irigoyen, M., Moscoso, P., and Giordano, S., 2015, A late eocene-early Oligocene transgressive event in the Golfo San Jorge basin: Palynological results and stratigraphic implications: Journal of South American Earth Sciences, v. 63, p. 293–309, doi:10.1016/j.jsames.2015.08.009.

Parras, A., Dix, G.R., and Griffin, M., 2012, Sr-isotope chronostratigraphy of Paleogene-

Neogene marine deposits: Austral Basin, southern Patagonia (Argentina): Journal of South American Earth Sciences, v. 37, p. 122–135.

Parras, A., Griffin, M., Feldmann, R., Casadío, S., Schweitzer, C., and Marenssi, S., 2008, Journal of South American Earth Sciences Correlation of marine beds based on Sr- and Ar-date determinations and faunal affinities across the Paleogene/Neogene boundary in southern Patagonia, Argentina: Journal of South American Earth Sciences, v. 26, p. 204–216, doi:10.1016/j.jsames.2008.03.006.

Pepper, M., Gehrels, G., Pullen, A., Ibanez-Mejia, M., Ward, K.M., and Kapp, P., 2016, Magmatic history and crustal genesis of western South America: Constraints from U-Pb ages and Hf isotopes of detrital zircons in modern rivers: Geosphere, v. 12, p. 1532–1555, doi:10.1130/GES01315.1.

Perez, N.D., and Horton, B.K., 2014, Oligocene-miocene deformational and depositional history of the andean hinterland basin in the northern altiplano Plateau, Southern Peru: Tectonics, v. 33, p. 1819–1847, doi:10.1002/2014TC003647.

Perkins, M.E., Fleagle, J.G., Heizler, M.T., Nash, B., Bown, T.M., Tauber, A. a, and Dozo, M.T., 2012, Tephrochronology of the Miocene Santa Cruz and Pinturas Formations, Argentina: Early Miocene Paleobiology in Patagonia: High-Latitude Paleocommunities of the Santa Cruz Formation, p. 23–40.

Ramos, V.A., 2005, Seismic ridge subduction and topography: Foreland deformation in the Patagonian Andes: Tectonophysics, v. 399, p. 73–86, doi:10.1016/j.tecto.2004.12.016.

Ramos, V.A., and Ghiglione, M.C., 2008, Tectonic Evolution of the Patagonian Andes: Developments in Quaternary Science, v. 11, p. 57–71, doi:10.1016/S1571-0866(07)10004-X.

Rehak, K., Bookhagen, B., Strecker, M.R., and Echtler, H.P., 2010, The topographic imprint of a transient climate episode: The western Andean flank between 15°5' and 41°5'S: Earth Surface Processes and Landforms, v. 35, p. 1516–1534, doi:10.1002/esp.1992.

Riccardi, A., and Rolleri, E., 1980, Cordillera Patagónica Austral: Academia Nacional de Ciencias, v. 2, p. 1173–1306.

Rodríguez Raising, M., 2010, Estratigrafía secuencial de los depósitos marinos y continentales del Eoceno – Oligoceno temprano de la cuenca Austral, suroeste de la provincia de Santa Cruz: Universidad Nacional del Sur, 202 p.

Roe, G.H., Whipple, K.X., and Fletcher, J.K., 2008, Feedbacks among climate, erosion, and tectonics in a critical wedge orogen: American Journal of Science, v. 308, p. 815–842, doi:10.2475/07.2008.01.

Romans, B.W., Fildani, A., Graham, S.A., Hubbard, S.M., and Covault, J.A., 2010, Importance of predecessor basin history on the sedimentary fill of a retroarc foreland basin: provenance analysis of the Cretaceous Magallanes: Basin Research, v. 22, p. 640–658, doi:10.1111/j.1365-2117.2009.00443.x.

Romans, B.W.W., Fildani, a., Hubbard, S.M.M., Covault, J. a. A., Fosdick, J.C.C., and Graham, S. a. A., 2011, Evolution of deep-water stratigraphic architecture, Magallanes Basin, Chile: Marine and Petroleum Geology, v. 28, p. 612–628, doi:10.1016/j.marpetgeo.2010.05.002.

Le Roux, J.P., Puratich, J., Mourgues, F.A., Oyarzún, J.L., Otero, R.A., Torres, T., and Hervé, F., 2010, Estuary deposits in the Río Baguales Formation (Chattian-Aquitanean), Magallanes Province, Chile: Andean Geology, v. 37, p. 329–344.

Sachse, V.F.F., Strozyk, F., Anka, Z., Rodriguez, J.F.F., and di Primio, R., 2015, The tectono-stratigraphic evolution of the Austral Basin and adjacent areas against the background of Andean tectonics, southern Argentina, South America: Basin Research, v. 26, p. 462–482, doi:10.1111/bre.12118.

Sánchez, A., Pavlishina, P., Godoy, E., Hervé, F., and Fanning, C.M., 2010, On the presence of Upper Paleocene rocks in the foreland succsion at Cabo Nariz, Tierra del Fuego, Chile: geology and new palynological and U-Pb data: Andean Geology, v. 37, p. 413–432.

Schmitt, J.G., and Steidtmann, J.R., 1990, Interior ramp-supported uplifts: Implications for sediment provenance in foreland basins: Geological Society of America Bulletin, v. 102, p. 494–201.

Schwartz, T.M., Fosdick, J.C., and Graham, S.A., 2016, Using detrital zircon U-Pb ages to calculate Late Cretaceous sedimentation rates in the Magallanes-Austral basin, Patagonia: Basin Research, v. 29, p. 725–746, doi:10.1111/bre.12198.

Schwartz, T.M., and Graham, S.A., 2015a, Stratigraphic architecture of a tide-influenced shelf-edge delta, Upper Cretaceous Dorotea Formation, Magallanes-Austral Basin, Patagonia: Sedimentology, v. 62, p. 1039–1077, http://doi.wiley.com/10.1111/sed.12176.

Schwartz, T.M., and Graham, S.A., 2015b, Stratigraphic architecture of a tide-influenced shelf-edge delta, Upper Cretaceous Dorotea Formation, Magallanes-Austral Basin, Patagonia: Sedimentology, v. 62, p. 1039–1077, doi:10.1111/sed.12176.

Schweitzer, C.E., Feldmann, R.M., Casadío, S., and Rodríguez Raising, M., 2012, Eocene decapod crustacea (thalassinidea and brachyura) from Patagonia, Argentina: Annals of Carnegie Museum, v. 80, p. 173–186, http://www.scopus.com/inward/record.url?eid=2-s2.0-84866259713&partnerID=40&md5=7944fae1d80175829a8dbfc8a5993452.

Sepkoski, J.J., 1996, Patterns of Phanerozoic Extinction: a Perspective from Global Data Bases, *in* Walliser, D.H. ed., Global Events and Event Stratigraphy in the Phanerozoic, Berlin, Springer, p. 35–51.

SERNAGEOMIN, 2003, Mapa Geológico de Chile: versión digital. Servicio Nacional de Geología y Minería, Publicación Geológica Digital, No. 4 (CD-ROM, versión 1.0).:

Sickmann, Z.T., Schwartz, T.M., and Graham, S.A., 2018, Refining stratigraphy and tectonic history using detrital zircon maximum depositional age: an example from the Cerro Fortaleza Formation, Austral Basin, southern Patagonia: Basin Research, v. 30, p. 708–729, doi:10.1111/bre.12272.

Simpson, G.D.H., 2006, Modelling interactions between fold-thrust belt deformation, foreland flexure and surface mass transport: Basin Research, v. 18, p. 125–143, doi:10.1111/j.1365-2117.2006.00287.x.

Sommerfield, C.K., and Wheatcroft, R.A., 2007, Late Holocene sediment accumulation on the northern California shelf: Oceanic, fluvial, and anthropogenic influences: Bulletin of the Geological Society of America, v. 119, p. 1120–1134, doi:10.1130/B26019.1.

Somoza, R., and Ghidella, M.E., 2012, Late Cretaceous to recent plate motions in western South America revisited: Earth and Planetary Science Letters, v. 331–332, p. 152–163, doi:10.1016/j.epsl.2012.03.003.

Stocchi, P. et al., 2013, Relative sea-level rise around East Antarctica during Oligocene glaciation: Nature Geoscience, v. 6, p. 380–384, doi:10.1038/NGEO1783.

Süssenberger, A., Schmidt, S.T., Wemmer, K., Baumgartner, L.P., and Grobéty, B., 2017, Timing and thermal evolution of fold-and-thrust belt formation in the Ultima Esperanza District, 51°S Chile : Constraints from K-Ar dating and illite characterization: Geological Society Of America Bulletin, v. 130, p. 975–998.

Ugalde, R.A., 2014, Contribución al conocimiento de la estratigrafia Cenozoica de La Sierra Baguales: La Formación Man Aike (“Las Flores”), Provincia de Ultima Esperanza, Magallanes: Universidad de Chile, 92 p.

Vento, B., Gandolfo, M.A., Nixon, K.C., and Prámparo, M., 2017, Paleofloristic assemblage from the Paleogene Río Guillermo Formation, Argentina: preliminary results of phylogenetic relationships of Nothofagus in South America: Historical Biology, v. 29, p. 93–107, doi:10.1080/08912963.2015.1136930.

Wilf, P., Cúneo, N.R., Johnson, K.R., Hicks, J.F., Wing, S.L., and Obradovich, J.D., 2003, High plant diversity in Eocene South America: evidence from Patagonia.: Science (New York, N.Y.), v. 300, p. 122–125, doi:10.1126/science.1080475.

Willett, S.D., 1999, Orogeny and orography: The effects of erosion on the structure of mountain belts: Journal of Geophysical Research, v. 104, p. 28957–28981, doi:10.1029/1999JB900248.

Zachos, J.C., Dickens, G.R., and Zeebe, R.E., 2008, An early Cenozoic perspective on greenhouse warming and carbon-cycle dynamics.: Nature, v. 451, p. 279–283, doi:10.1038/nature06588.

Zachos, J., Pagani, M., Sloan, L., Thomas, E., and Billups, K., 2001, Trends, rhythms, and aberrations in global climate 65 Ma to present.: Science, v. 292, p. 686–93, doi:10.1126/science.1059412.

TABLE CAPTIONS

Table 1. Sample information and calculated maximum depositional ages from the Magallanes Basin for detrital zircon U-Pb LA-ICP-MS geochronology.

FIGURE CAPTIONS

Figure 1. (A) Tectonic setting of the Magallanes Basin and other Cenozoic depocenters (yellow) in relation to key southern plate boundary features (after Galeazzi, 1998; Ghiglione et al., 2010; Fosdick et al., 2011). Global Multi-Resolution Topography (GMRT) base map from GeoMapApp©. Black stars denote stratigraphic areas discussed in the text: CC – Cerro Castillo, SJ – San Julian. NP – Nazca plate; NSR – North Scotia Ridge; MFFZ – Magallanes-Fagnano Fault Zone; SFZ – Shackleton Fracture Zone. (B) Location of the Cerro Castillo – Cancha Carrera study area within the Cenozoic Magallanes-Austral Basin outcrop belt along the eastern margins of the Patagonian thrust belt. Geologic map compiled from Malumián et al. (2000), SERNAGEOMIN (2003), and Fosdick et al. (2011). Zircon crystallization ages are summarized from igneous and recycled sediment sources (Fosdick et al., 2015 and references therein).

Figure 2. Detrital zircon U-Pb geochronology data compiled by formation (<600 Ma only), showing probability density plots of Upper Cretaceous through lower Miocene stratigraphy. For each formation, N refers to the number of individual samples included in the formation, followed by number of total grains analyzed. Published data from the Santa Cruz, Dorotea, Tres Pasos, and Punta Barrosa Formations are included for comparison (Fildani et al., 2003; Romans et al., 2010; Bernhardt et al., 2012; Fosdick et al., 2015). Note break in scale at 360-600 Ma and change of scale after 600 Ma. Intrusive age groups after Hervé et al. (2007): N = Neogene, P = Paleogene, K1 = Cretaceous I, K2 = Cretaceous II, K3 = Cretaceous III, and J = Jurassic. PZ = Paleozoic. We identify ‘K4’ and ‘P2’ age groups in our detrital datasets.

Figure 3. Maximum depositional ages (MDA) interpreted from the youngest detrital zircon U-Pb data from each sample (individual analyses shown at 2σ uncertainty). MDA are the error-weighted mean age (± 2σ uncertainty) of all grains (n) that define the youngest age cluster represented by the horizontal gray bars.

Figure 4. Changes in relative proportions of zircon age groups for pre-Cenozoic age groups. Results show upsection rise and subsequent loss of Jurassic – Early Cretaceous (J-K1) grains, a progressive loss of Paleozoic grains, and an overall increase in Paleogene igneous sources. The largest shift in provenance signature occurred across the Paleocene Cerro Dorotea Formation - middle Eocene Río Turbio Formation boundary.

Figure 5. Summary of new depositional age constraints and paleoenvironmental context in the Magallanes Basin near 51°S. Cenozoic stratigraphy and revised timing of sedimentation based on new maximum depositional ages (MDA) calculated from youngest detrital zircon U-Pb age cluster from each sample.

Figure 6. Implications for revised timing of sedimentation of the middle Cenozoic Magallanes-Austral Basin strata compared to changes in regional tectonics (Breitsprecher and Thorkelson, 2009; Lagabrielle et al., 2009; Fosdick et al., 2011), plate convergence rate (Somoza and Ghidella, 2012), global climate (Zachos et al., 2008), and eustatic sea level (Miller, 2008). Published chronostratigraphy of proximal foothills compiled from Malumián et al. (2000), Malumián and Náñez, (2011), Perkins et al. (2012), and references therein. Chronostratigraphy of the San Julián sector of the Atlantic coast from Parras et al. (2008) and (2012). New age estimates and sediment provenance highlight (1) isolation of Jurassic and Paleozoic zircon sources and disruption of the foreland basin system across the Paleogene foreland unconformity, (2) a potential foreland younging transgression caused by flexural deepening during Tenerife thrusting and synchronous basin subsidence in Tierra del Fuego, and (3) accelerated sediment supply of the Río Guillermo Formation linked to retroarc deformation and unroofing along the El Ríncon thrusts.

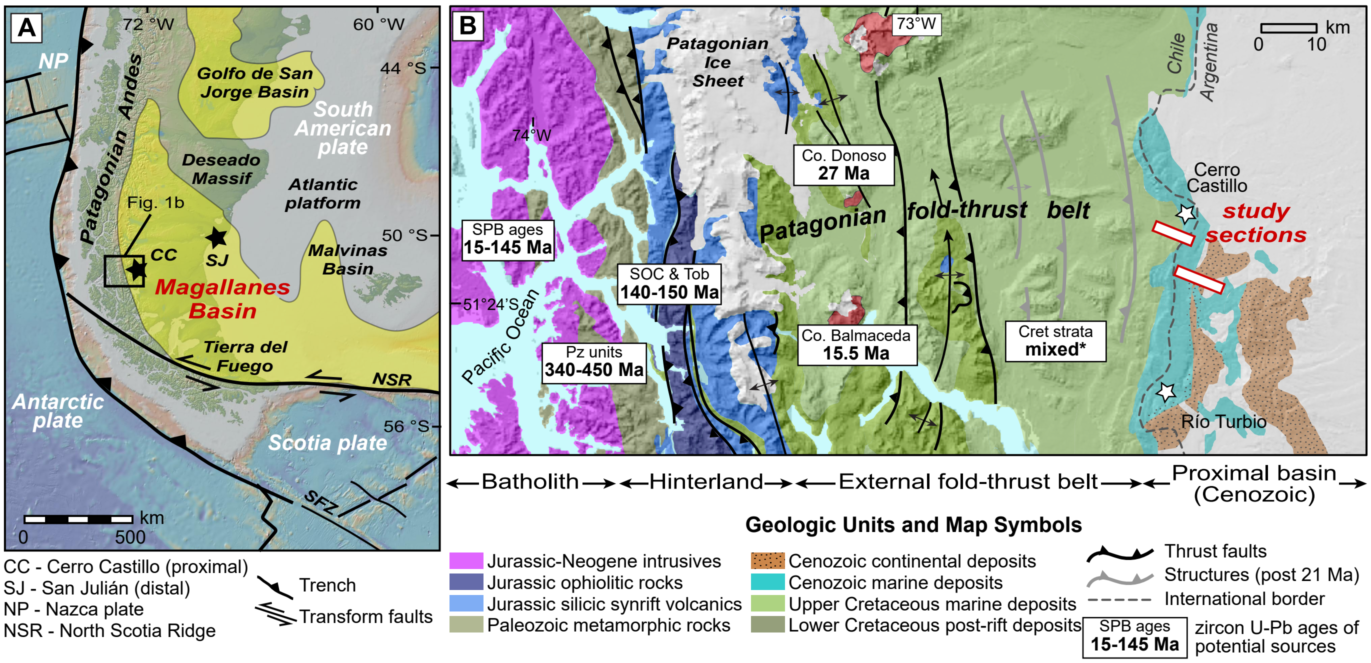

A
72 °W
60 °W
NP
44 °S
Golfo de San Jorge Basin
Patagonian Andes
South American plate
Deseado Massif
Atlantic platform
Fig. 1b
50 °S
CC
SJ
Malvinas Basin
Magallanes Basin
Tierra del Fuego
NSR
Antarctic plate
56 °S
Scotia plate
SFZ
km
0
500
CC - Cerro Castillo (proximal)
SJ - San Julián (distal)
NP - Nazca plate
NSR - North Scotia Ridge
Trench
Transform faults
B
Patagonian Ice Sheet
73°W
km
0
10
Chile
Argentina
74°W
Co. Donoso
27 Ma
Cerro Castillo
study sections
Patagonian
fold-thrust
belt
SPB ages
15-145 Ma
SOC & Tob
140-150 Ma
51°24'S
Pacific Ocean
Co. Balmaceda
15.5 Ma
Cret strata
mixed*
Pz units
340-450 Ma
Río Turbio
Batholith
Hinterland
External fold-thrust belt
Proximal basin (Cenozoic)
Geologic Units and Map Symbols
Jurassic-Neogene intrusives
Jurassic ophiolitic rocks
Jurassic silicic synrift volcanics
Paleozoic metamorphic rocks
Cenozoic continental deposits
Cenozoic marine deposits
Upper Cretaceous marine deposits
Lower Cretaceous post-rift deposits
Thrust faults
Structures (post 21 Ma)
International border
SPB ages
15-145 Ma
zircon U-Pb ages of potential sources

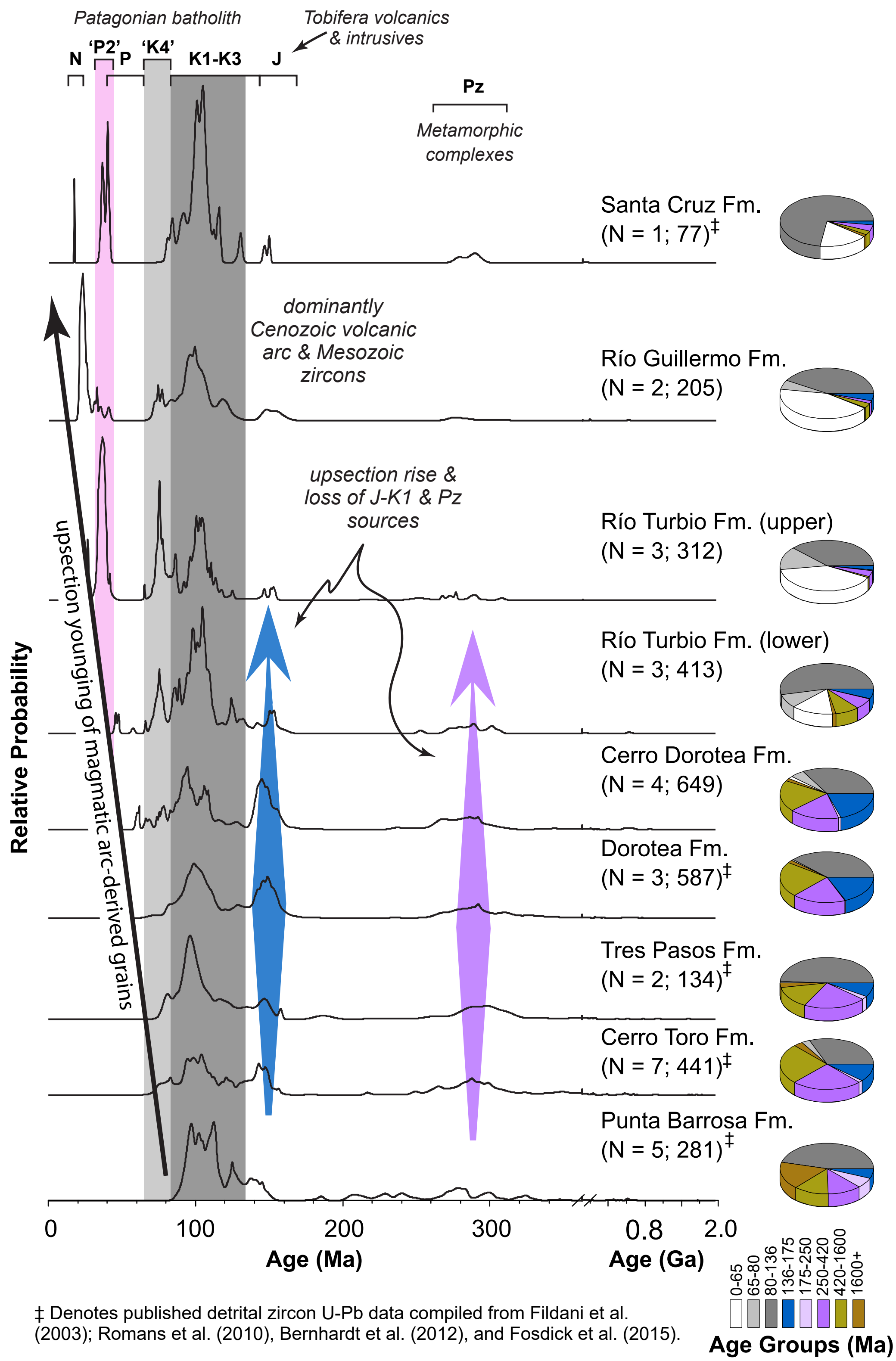

Figure 2. Detrital zircon U-Pb geochronology data compiled by formation (<600 Ma only), showing probability density plots of Upper Cretaceous through lower Miocene stratigraphy. For each formation, N refers to the number of individual samples included in the formation, followed by number of total grains analyzed. Published data from the Santa Cruz, Dorotea, Tres Pasos, and Punta Barrosa Formations are included for comparison (Fildani et al., 2003; Romans et al., 2010; Bernhardt et al., 2012; Fosdick et al., 2015). Note break in scale at 360-600 Ma and change of scale after 600 Ma. Intrusive age groups after Hervé et al. (2007): N = Neogene, P = Paleogene, K1 = Cretaceous I, K2 = Cretaceous II, K3 = Cretaceous III, and J = Jurassic. PZ = Paleozoic. We identify 'K4' and 'P2' age groups in our detrital datasets.

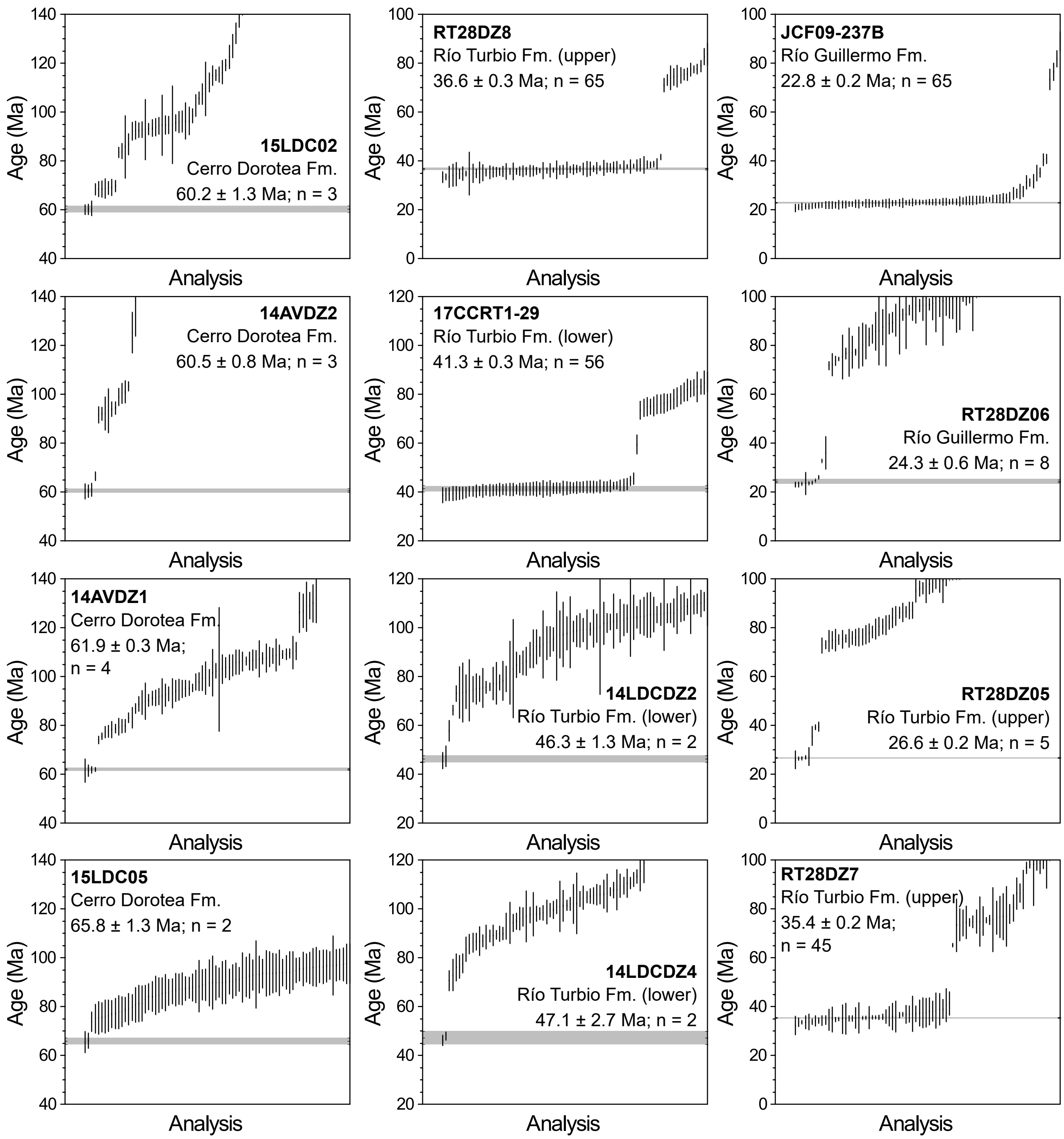

Figure 3. Maximum depositional ages (MDA) interpreted from the youngest detrital zircon U-Pb data from each sample (individual analyses shown at 2σ uncertainty). MDA are the error-weighted mean age (± 2σ uncertainty) of all grains (n) that define the youngest age cluster represented by the horizontal gray bars.

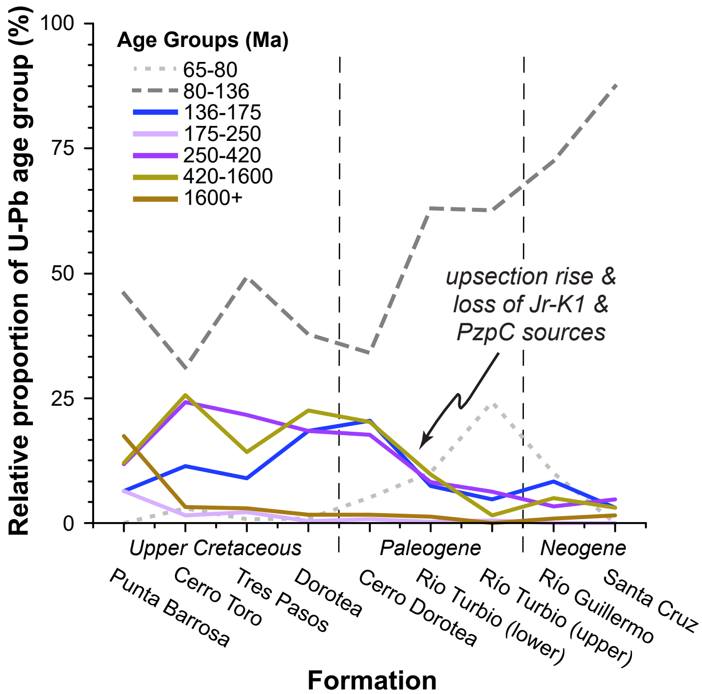

Figure 4. Changes in relative proportions of zircon age groups for pre-Cenozoic age groups. Results show upsection rise and subsequent loss of Jurassic – Early Cretaceous (J-K1) grains, a progressive loss of Paleozoic grains, and an overall increase in Paleogene igneous sources. The largest shift in provenance signature occurred across the Paleocene Cerro Dorotea Formation - middle Eocene Río Turbio Formation boundary.

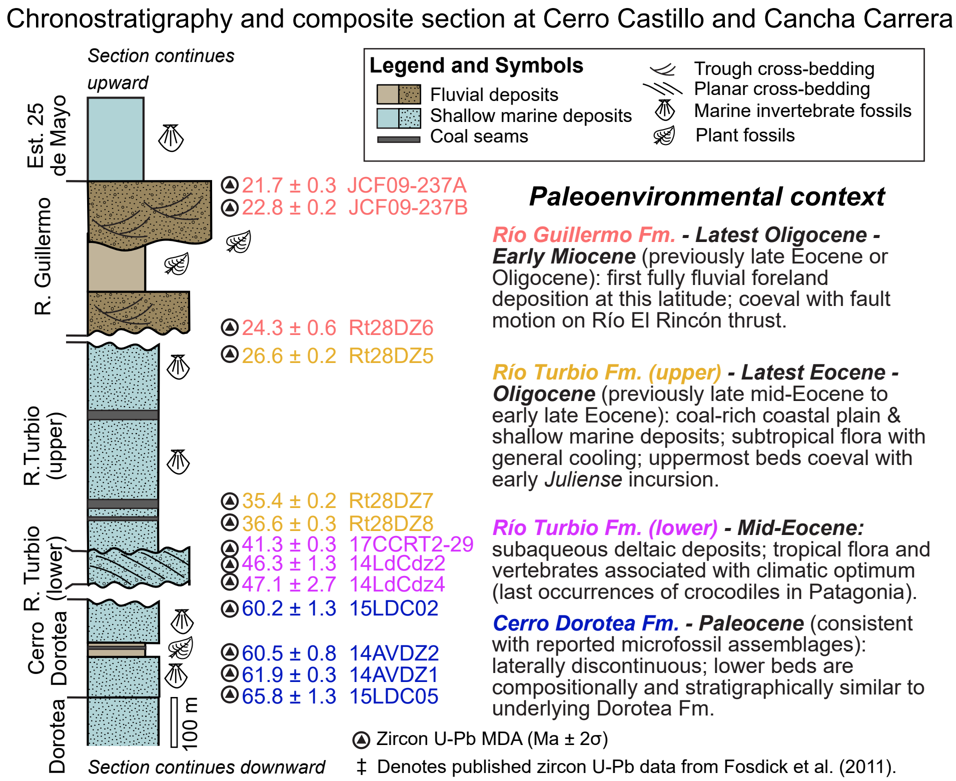

Figure 5. Summary of new depositional age constraints and paleoenvironmental context in the Magallanes Basin near 51°S. Cenozoic stratigraphy and revised timing of sedimentation based on new maximum depositional ages (MDA) calculated from youngest detrital zircon U-Pb age cluster from each sample.

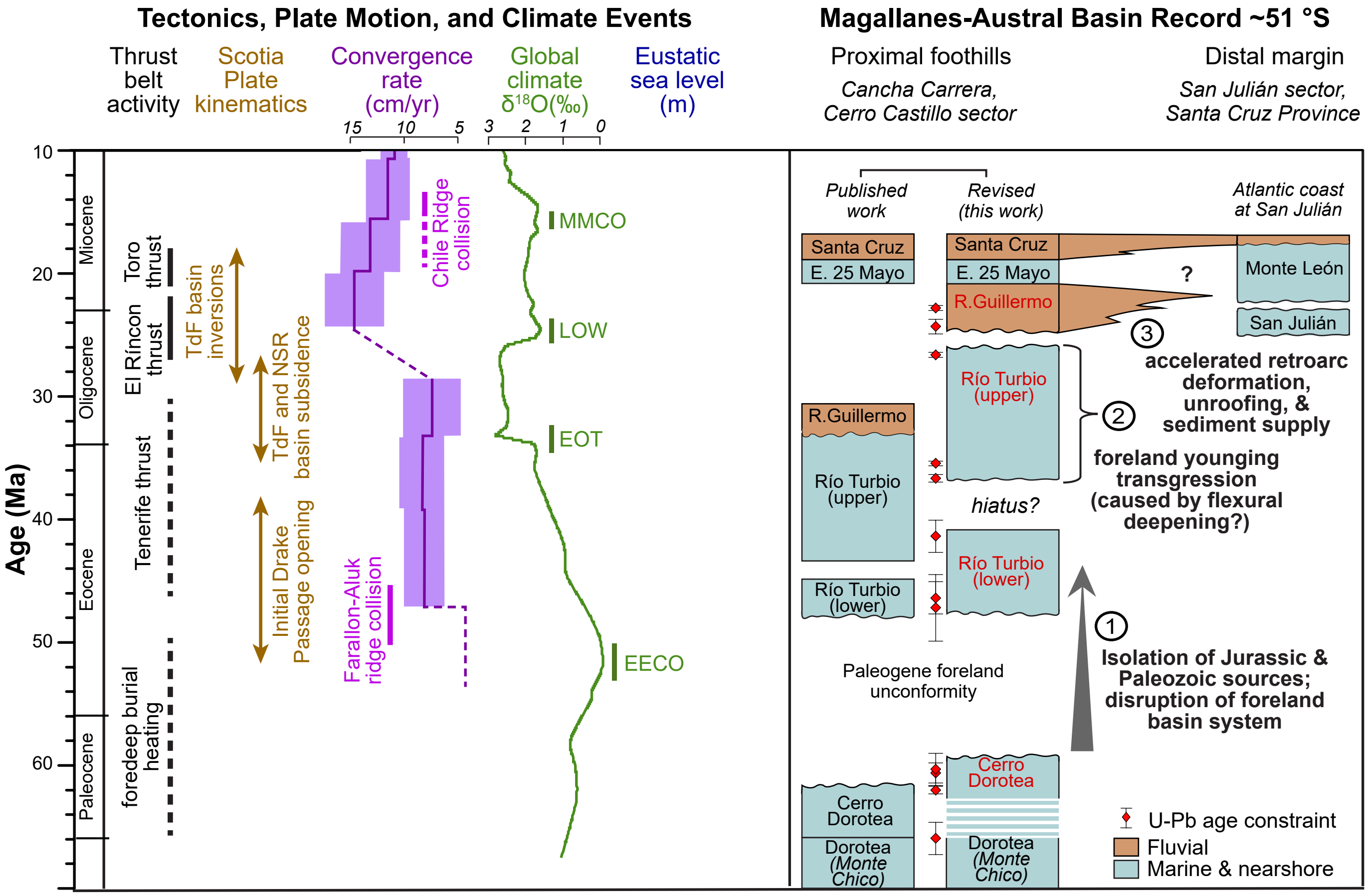

Figure 6. Implications for revised timing of sedimentation of the middle Cenozoic Magallanes-Austral Basin strata compared to changes in regional tectonics (Breitsprecher and Thorkelson, 2009; Lagabrielle et al., 2009; Fosdick et al., 2011), plate convergence rate (Somoza and Ghidella, 2012), global climate (Zachos et al., 2008), and eustatic sea level (Miller, 2008). Published chronostratigraphy of proximal foothills compiled from Malumián et al. (2000), Malumián and Náñez, (2011), Perkins et al. (2012), and references therein. Chronostratigraphy of the San Julián sector of the Atlantic coast from Parras et al. (2008) and (2012). New age estimates and sediment provenance highlight (1) isolation of Jurassic and Paleozoic zircon sources and disruption of the foreland basin system across the Paleogene foreland unconformity, (2) a potential foreland younging transgression caused by flexural deepening during Tenerife thrusting and synchronous basin subsidence in Tierra del Fuego, and (3) accelerated sediment supply of the Río Guillermo Formation linked to retroarc deformation and unroofing along the El Víncon thrusts.

TABLE 1. SAMPLE INFORMATION AND CALCULATED MAXIMUM DEPOSITIONAL AGES FROM THE MAGALLANES BASIN FOR DETRITAL ZIRCON U-Pb LA-ICP-MS GEOCHRONOLOGY

Sample	Formation	Latitude (°N)	Longitude (°W)	Elevation (m)	# grains analyzed	Interpreted maximum depositional age (± 2σ)
JCF09-237B	Río Guillermo	-51.30338	-72.18670	389	115	22.8 ± 0.2 Ma (n = 65)
Rt28DZ6	Río Guillermo	-51.31163	-72.22042	346	94	24.3 ± 0.6 Ma (n = 8)
Rt28DZ5	Río Turbio (upper)	-51.31373	-72.21932	323	103	26.6 ± 0.5 Ma (n = 5)
Rt28DZ7	Río Turbio (upper)	-51.29761	-72.23581	349	101	35.4 ± 0.2 Ma (n = 45)
Rt28DZ8	Río Turbio (upper)	-51.29667	-72.23819	282	110	36.6 ± 0.3 Ma (n = 65)
17CCRT2-29	Río Turbio (lower)	-51.31735	-72.29126	464	157	41.3 ± 0.3 Ma (n = 56)
14LdCdz2	Río Turbio (lower)	-51.28071	-72.28936	443	106	46.3 ± 1.3 Ma (n = 2)
14LdCdz4	Río Turbio (lower)	-51.27997	-72.28916	411	108	47.1 ± 2.7 Ma (n = 2)
15LDC02/14DZ3	Cerro Dorotea	-51.28001	-72.28927	351	227	60.2 ± 1.3 Ma (n = 3)
14AVDZ2	Cerro Dorotea	-51.28475	-72.30764	433	107	60.5 ± 0.8 Ma (n = 3)
14AVDZ1	Cerro Dorotea	-51.28473	-72.30828	434	103	61.9 ± 0.3 Ma (n = 4)
15LDC05	Cerro Dorotea	-51.27793	-72.31254	312	212	65.8 ± 1.3 Ma (n = 2)

Revised timing of Cenozoic Atlantic incursions and changing hinterland sediment sources during southern Patagonian orogenesis

Data Repository

U-Pb geochronologic analyses of detrital zircon (Nu HR ICPMS)

Detrital zircons were extracted from ~5 kg medium-grained sandstone hand-samples using standard mineral separation techniques at the ZirChron, LLC. (Tucson, Arizona), including crushing and grinding, fractionation of magnetic minerals with a Frantz isodynamic magnetic separator, and settling through heavy liquids to exclude phases with densities less than 3.3 g/cm^3. Final zircon separates were mounted in epoxy resin together with fragments of the Sri Lanka standard zircon. The mounts are polished to a depth of ~20 μm, imaged, and cleaned prior to isotopic analysis.

U-Pb geochronology of zircons is conducted by laser ablation multicollector inductively coupled plasma mass spectrometry (LA-MC-ICPMS) at the Arizona LaserChron Center (Gehrels et al., 2008; Gehrels, 2012). The analyses involve ablation of zircon with a Photon Machines Analyte G2 excimer laser using a spot diameter of 30 μm. The ablated material is carried in helium into the plasma source of a Nu HR ICPMS, which is equipped with a flight tube of sufficient width that U, Th, and Pb isotopes are measured simultaneously. All measurements are made in static mode, using Faraday detectors with 3x10^{11} ohm resistors for ^{238}U, ^{232}Th, ^{208}Pb-^{206}Pb, and discrete dynode ion counters for ^{204}Pb and ^{202}Hg. Ion yields are ~0.8 mv per ppm. Each analysis consists of one 15-second integration on peaks with the laser off (for backgrounds), 15 one-second integrations with the laser firing, and a 30 second delay to purge the previous sample and prepare for the next analysis. The ablation pit is ~15 μm in depth.

For each analysis, the errors in determining ^{206}Pb/^{238}U and ^{206}Pb/^{204}Pb result in a measurement error of ~1-2% (at 2σ level) in the ^{206}Pb/^{238}U age. The errors in measurement of ^{206}Pb/^{207}Pb and ^{206}Pb/^{204}Pb also result in ~1-2% (at 2σ level) uncertainty in age for grains that are >1.0 Ga, but are substantially larger for younger grains due to low intensity of the ^{207}Pb signal. For most analyses, the cross-over in precision of ^{206}Pb/^{238}U and ^{206}Pb/^{207}Pb ages occurs at ~1.0 Ga. ^{204}Hg interference with ^{204}Pb is accounted for measurement of ^{202}Hg during laser ablation and subtraction of ^{204}Hg according to the natural ^{202}Hg/^{204}Hg of 4.35. This Hg is correction is not significant for most analyses because our Hg backgrounds are low (generally ~150 cps at mass 204). Common Pb correction is accomplished by using the Hg-corrected ^{204}Pb and assuming an initial Pb composition (Stacey and Kramers, 1975). Uncertainties of 1.5 for ^{206}Pb/^{204}Pb and 0.3 for ^{207}Pb/^{204}Pb are applied to these compositional values based on the variation in Pb isotopic composition in modern crystal rocks. Inter-element fractionation of Pb/U is generally ~5%, whereas apparent fractionation of Pb isotopes is generally <0.2%. In-run analysis of fragments of a large zircon crystal (generally every fifth measurement) with known age of 563.5 ± 3.2 Ma (2σ error) is used to correct for this fractionation. The uncertainty resulting from the calibration correction is generally 1-2% (2σ) for both ^{206}Pb/^{207}Pb and ^{206}Pb/^{238}U ages. Concentrations of U and Th are calibrated relative to Sri Lanka zircon, which contains ~518 ppm of U and 68 ppm Th.

The analytical data are reported in Table A1. Preferred calculated U-Pb ages use the ^{204}Pb corrected ^{206}Pb/^{238}U ratio for <1.0 Ga grains and the ^{204}Pb corrected ^{206}Pb/^{207}Pb ratio for >900 Ma grains. Uncertainties shown in these tables are at the 1σ level, and include only measurement errors. Analyses that are >20% discordant or >5% reverse discordant (by comparison of ^{206}Pb/^{238}U and ^{206}Pb/^{207}Pb ages) were excluded from provenance interpretations and maximum depositional age calculations. Pb*/U concordia diagrams (Fig. A1) and probability density plots (Figs. A2 and A3) were generated using the routines in Isoplot (Ludwig, 2008). The age-probability diagrams show each age and its uncertainty (for measurement error only) as a normal distribution, and sum all ages from a sample into a single curve. For samples that yielded youngest age groups that could represent conceivable maximum depositional ages, we calculated error-weighted mean ages (Table 1) based on the following criteria: age clusters contained at least 2 overlapping concordant grains at 2σ uncertainty. For published samples from collected within the latitude of our study area from the Punta Barrosa, Cerro Toro, Tres Pasos, Dorotea, and Santa Cruz Formations (Fig. 2 and Fig. 4), we recalculated relative probability density curves from published detrital zircon U-Pb geochronological data (Fildani et al., 2003; Romans et al., 2010; Bernhardt et al., 2012; Fosdick et al., 2015): Punta Barrosa Formation samples included in data comparison are: *Pb0104, 2/21-3, 2/6-3, 3/5-3*, and *3/11-3* (Fildani et al., 2003). Cerro Toro Formation samples included in data comparison are: *CC* and *VC* (Romans et al., 2010) and *SS-Ndskld, CB-C, SdT-Co, SdT-Wc, SS_PehoeA* (Bernhardt et al., 2012). Tres Pasos Formation samples included in data comparison are: *F04* and *F05-1* (Romans et al., 2010).

Dorotea Formation samples included in data comparison are: *CCS-01* and *CM-1* (Romans et al., 2010) and *JCF09-226* (Fosdick et al., 2015). Santa Cruz Formation samples included in data comparison are: *JCF09-235* (Fosdick et al., 2015).

REFERENCES

Bernhardt, A., Jobe, Z.R., Grove, M., and Lowe, D.R., 2012, Palaeogeography and diachronous infill of an ancient deep-marine foreland basin, Upper Cretaceous Cerro Toro Formation, Magallanes Basin: Basin Research, v. 24, p. 269–294.

Fildani, A., Cope, T.D., Graham, S.A., and Wooden, J.L., 2003, Initiation of the Magallanes foreland basin: Timing of the southernmost Patagonian Andes orogeny revised by detrital zircon provenance analysis: Geology, v. 31, p. 1081–1084.

Fosdick, J.C., Grove, M., Graham, S.A., Hourigan, J.K., Lovera, O., and Romans, B.W., 2015, Detrital thermochronologic record of burial heating and sediment recycling in the Magallanes foreland basin, Patagonian Andes: Basin Research, v. 27, p. 546–572.

Gehrels, G., 2012, Detrital Zircon U-Pb Geochronology: Current Methods and New Opportunities: Tectonics of Sedimentary Basins, p. 45–62, doi:10.1002/9781444347166.ch2.

Gehrels, G.E., Valencia, V.A., and Ruiz, J., 2008, Enhanced precision, accuracy, efficiency, and spatial resolution of U-Pb ages by laser ablation-multicollector-inductively coupled plasma-mass spectrometry: Geochemistry, Geophysics, Geosystems, v. 9, p. 1–13.

Ludwig, K.R., 2008, User's Manual for Isoplot 3.60 - A Geochronological Toolkit for Microsoft Excel: Berkeley Geochronology Center Special Publication, v. 4, p. 77.

Romans, B.W., Fildani, A., Graham, S.A., Hubbard, S.M., and Covault, J.A., 2010, Importance of predecessor basin history on the sedimentary fill of a retroarc foreland basin: provenance analysis of the Cretaceous Magallanes: Basin Research, v. 22, p. 640–658.

Stacey, J.S., and Kramers, J.D., 1975, Approximation of terrestrial lead on a subset of magmatic rocks and isotope evolution by a two-stage model: Earth and Planetary Science Letters, v. 26, p. 207–221.

TABLES

Table A1. Zircon U-Pb LA-MC-ICPMS geochronological data.

FIGURES

Figure A1. Zircon U-Pb concordia diagrams for individual samples. Ellipses show 2σ uncertainty. n denotes the total number of analyzed grains per sample.

Figure A2. Relative probability plots of detrital zircon U-Pb ages for individual samples (0 to 2500 Ma). n denotes the total number of analyzed grains per sample.

Figure A3. Relative probability plots of detrital zircon U-Pb ages for individual samples (0 to 600 Ma).

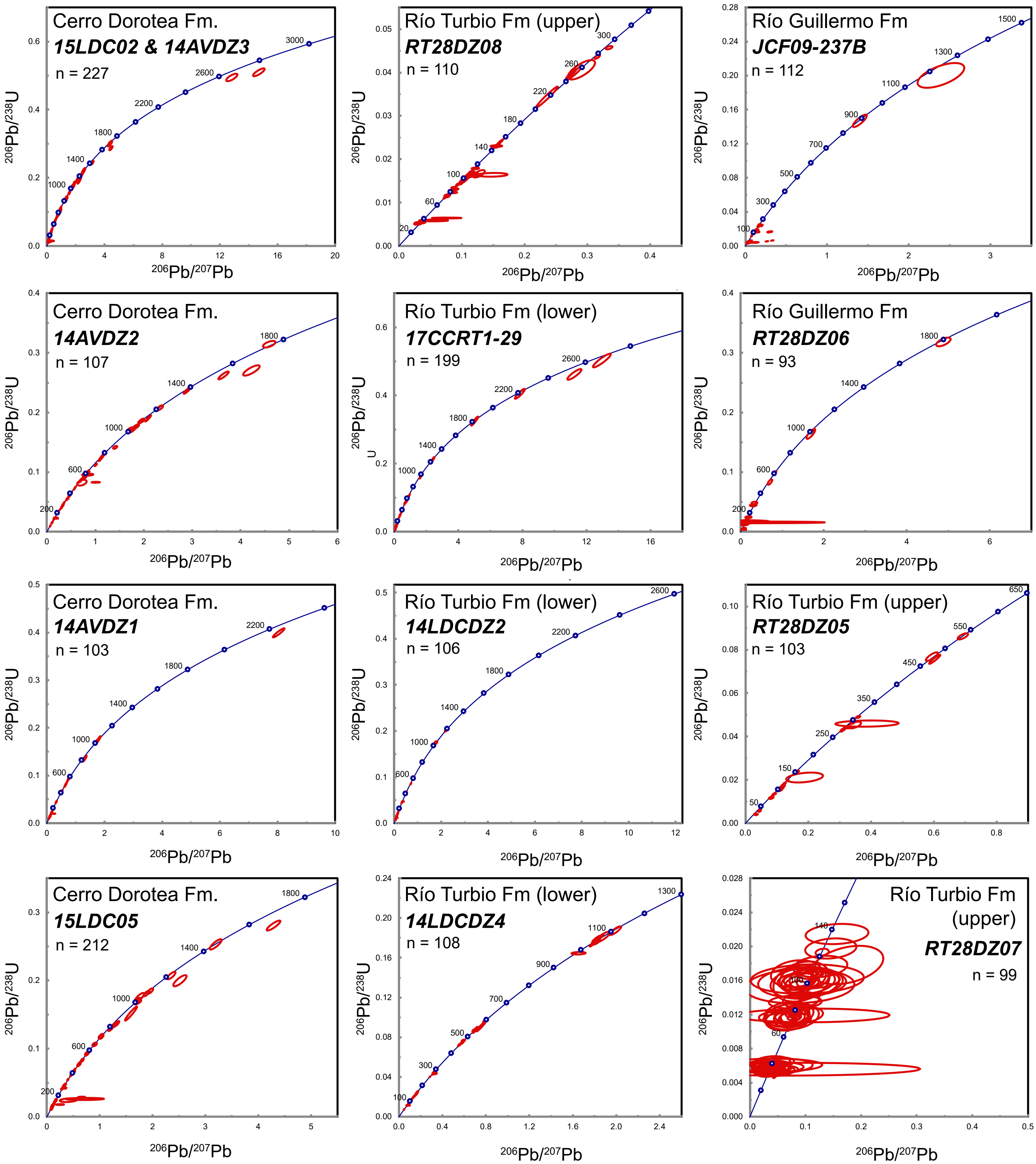

Figure A1. Zircon U-Pb concordia diagrams for individual samples. Ellipses show 2σ uncertainty. n denotes the total number of analyzed grains per sample.

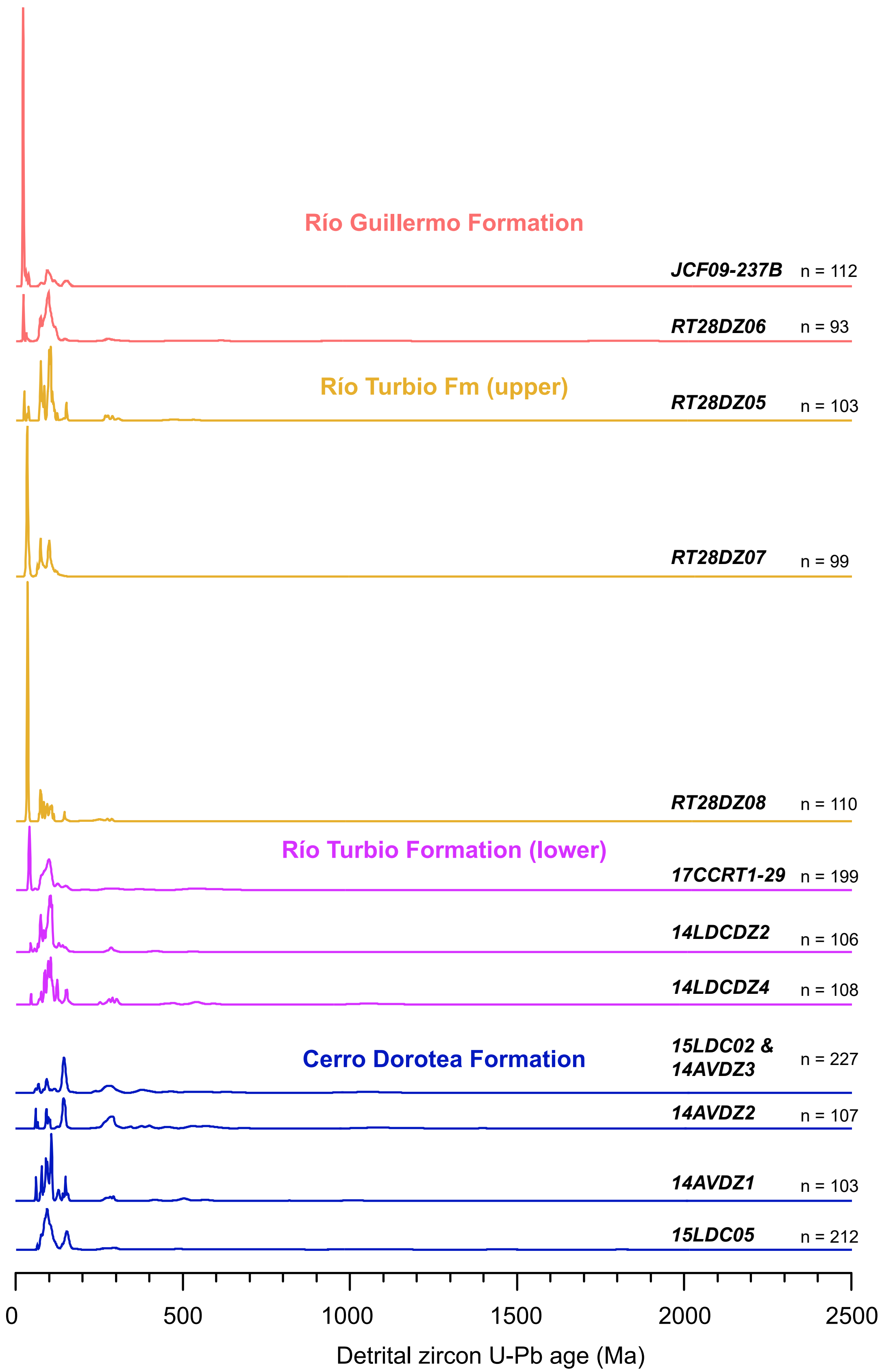

Figure A2. Relative probability plots of detrital zircon U-Pb ages for individual samples (0 to 2500 Ma). n denotes total number of analyzed grains per sample

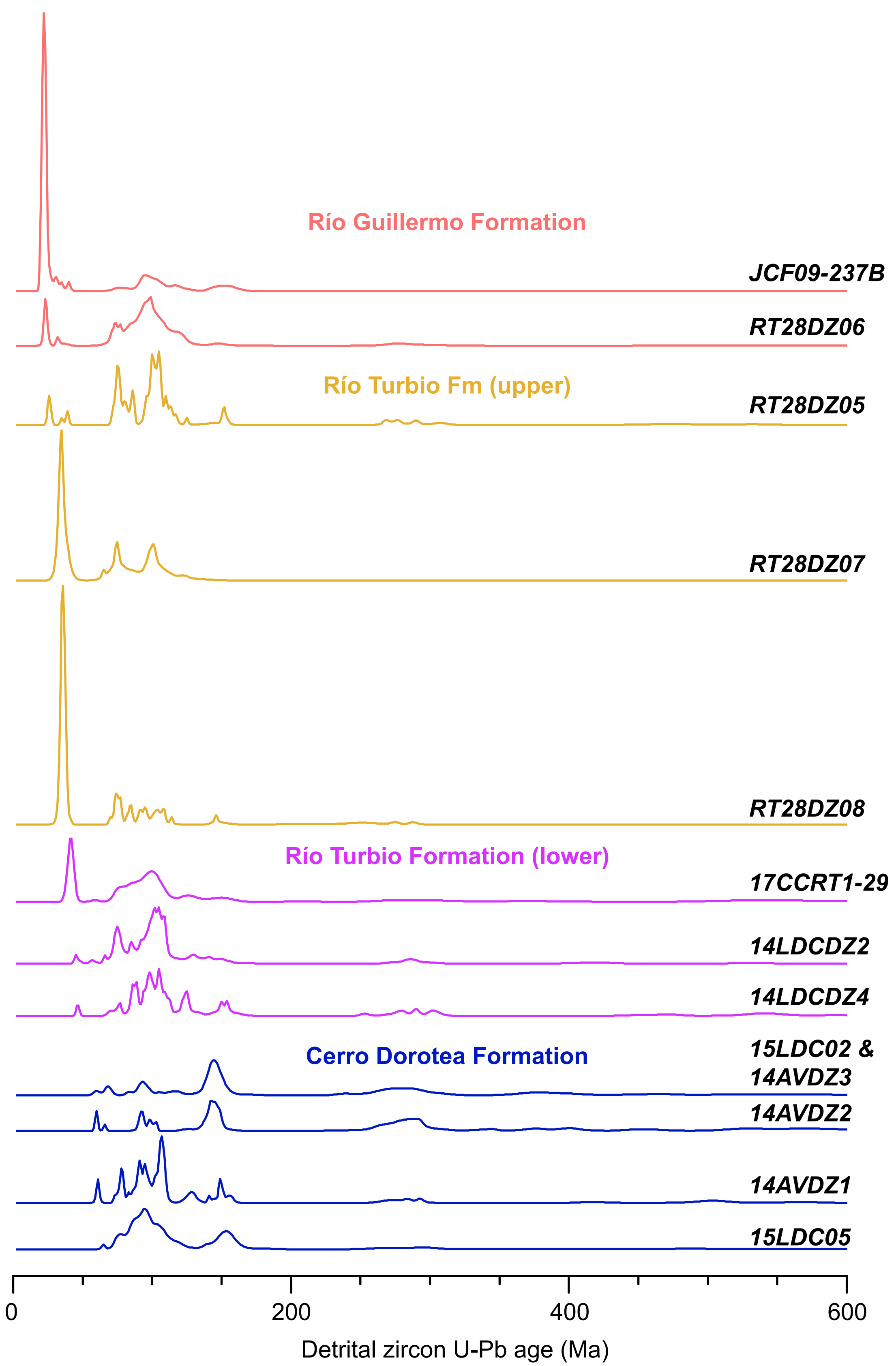

Figure A3. Relative probability plots of detrital zircon U-Pb ages for individual samples (0 to 600 Ma).